Data-driven exploration of the variability, controls and future changes of dimethyl sulfide in the global surface ocean

Shengqian Zhou[1], Ying Chen[1,2*], Fanghui Wang[1], Yang Bao[1], Guipeng Yang[3,4,5], Honghai Zhang[3,4,5], Yan Zhang[1,2], Zongjun Xu[1]

[1]Shanghai Key Laboratory of Atmospheric Particle Pollution Prevention, Department of Environmental Science & Engineering, and Institute of Atmospheric Sciences, Fudan University, Shanghai 200438, China.

[2]Institute of Eco-Chongming (IEC), Shanghai 202162, China.

[3]Frontiers Science Center for Deep Ocean Multispheres and Earth System, and Key Laboratory of Marine Chemistry Theory and Technology, Ministry of Education, Ocean University of China, Qingdao, Shandong 266100, China.

[4]Laboratory for Marine Ecology and Environmental Science, Qingdao National Laboratory for Marine Science and Technology, Qingdao, Shandong 266071, China.

[5]College of Chemistry and Chemical Engineering, Ocean University of China, Qingdao, Shandong 266100, China.

[*]Corresponding author: Ying Chen (yingchen@fudan.edu.cn)

Key Points:

- Machine learning can well capture the variability of dimethyl sulfide and unravel its relationships with environmental factors
- Nutrients and temperature are also crucial factors influencing dimethyl sulfide variations in the mid- and low-latitude open oceans
- The future changes of dimethyl sulfide concentration and emission have large spatial disparities and their global averages slightly decline

Abstract

As the largest natural source of sulfur-containing gases into the atmosphere, ocean organism-derived dimethyl sulfide (DMS) has been considered to play a critical role in the Earth's climate system. Yet there are great uncertainties in modeling the spatiotemporal variations of DMS and incomplete knowledge of influencing factors in different oceanic regions. Moreover, little is known about the future change of global DMS, which limits our understanding of the feedback of marine ecosystem to climate change. Here we develop an artificial neural network model and combine data mining approaches to address these issues. Phytoplankton biomass and salinity are currently predominant factors associated with DMS variability in the coastal and Arctic regions, respectively. In the mid- and low-latitude open oceans, nutrients and temperature are also crucial factors in addition to radiation and mixed layer depth, and their relationships with DMS show reversals when passing certain thresholds. Although the global average DMS concentration and emission slightly decline from 2005 to 2100, they may change considerably in specific regions. In contrast to the DMS decreases in the low-latitudes mainly related with phosphate reduction and temperature rise and in the North Atlantic subpolar gyre attributed to salinity decline, warming will cause DMS increase in the Southern Ocean and sea ice loss will dramatically enhance DMS emission in the Arctic. Although the global negative feedback loop between oceanic DMS and climate may not operate, the future spatial redistribution of DMS may lead to the change in cloud cover pattern and significantly affect regional climate.

Plain Language Summary

Dimethyl sulfide (DMS) mainly from marine biota is a key precursor of sulfate aerosols generating cooling effect on Earth's climate, but the response of DMS to global warming is highly uncertain with limited numbers of studies showing discrepant results. Based on decades-long sea surface DMS observations, we established a machine learning model to systematically explore the variabilities of DMS and their relationships with different environmental variables across global ocean. Then the future changes of DMS are projected and the dominant positive or negative factors are identified. The DMS concentration and emission present overall slight decreases in the 21st century, and their changes and causes have huge spatial disparities. The negative feedback of DMS to climate warming may not exist on a global scale but the spatial pattern shift may have a significant impact on regional climate. This work provides new insights into DMS biogeochemistry from a different perspective compared to conventional models, which helps to promote our understanding of the role of DMS in changing climate.

1 Introduction

Dimethyl sulfide (DMS) mostly produced by ocean biota accounts for more than half of natural sulfur emissions and contributes substantially to sulfur dioxide in the troposphere (Andreae, 1990; Sheng et al., 2015) which can be oxidized to sulfuric acid and form sulfate aerosols (Barnes et al., 2006; Hoffmann et al., 2016). Sulfate aerosols play an important role in mitigation of global warming by both scattering solar radiation and altering cloud condensation nuclei (CCN) and albedo (Masson-Delmotte et al., 2021). Recent studies have proven that CCN over remote oceans and polar regions are primarily composed of non-sea-salt sulfate (nss-SO_4^{2-}) (Park et al., 2021; Quinn et al., 2017). Given 70% coverage of the Earth's surface by the ocean and weak influence of anthropogenic SO_2 over open oceans, marine biogenic DMS can be the most important source of nss-SO_4^{2-} and regulates regional and global climate (McCoy et al., 2015). Accordingly, DMS has been suggested to be the key substance in the postulated negative

feedback of marine phytoplankton to climate warming (the "CLAW" hypothesis) (Charlson et al., 1987). However, there are still many knowledge gaps in testing the "CLAW" hypothesis (Quinn and Bates, 2011), and how oceanic DMS will respond to global warming is one of the most crucial puzzles. Therefore, accurate simulation of spatiotemporal variations of DMS in global oceans is required for understanding current atmospheric chemistry and climate system, and the prediction and attribution of DMS future trends are of great help for reducing the uncertainty of our knowledge about climate change.

Many researches have attempted to explore the oceanic DMS dynamics but found that DMS production and consumption mechanisms are more complex than expected. The major precursor of DMS, dimethylsulfoniopropionate (DMSP), is synthesized mainly by phytoplankton in the photic zone and plays a variety of physiological functions in algal cells (McParland and Levine, 2018; Stefels, 2000; Sunda et al., 2002). The DMSP yield differs dramatically among algal species with the high-yielding Haptophytes and Dinoflagellates relative to Cyanobacteria and diatoms (Keller et al., 1989; Stefels et al., 2007), and DMS can be produced through DMSP intracellular and extracellular cleavage by both algae and bacteria (Alcolombri et al., 2015; Zhang et al., 2019). Therefore, the oceanic DMS produced via multiple pathways can be affected by many biotic and abiotic factors, including temperature, salinity, solar radiation, mixed layer depth (MLD), nutrients, oxygen, acidity, etc. (Omori et al., 2015; Simó and Pedrós-Alió, 1999; Six et al., 2013; Stefels, 2000; Stefels et al., 2007; Vallina and Simó, 2007; Zindler et al., 2014). In addition, seawater DMS has multiple removal pathways (bacterial consumption, photodegradation, sea-to-air ventilation, etc.), further complicating the DMS cycling (Stefels et al., 2007). Tesdal et al. (2016) have evaluated diverse approaches for estimating the DMS variability in global ocean surface, and found great difference among the results regardless of data-based climatologies, empirical models or process-embedded prognostic models. In addition to the large uncertainty in mapping DMS distribution, the understanding of its controlling factors and future changes in different regions is more challenging, as a result of potential inconformity on different spatial and temporal scales. For example, the dominant controlling factor of DMS variation on a global scale may be less important in a specific region. Besides, the key factor driving the seasonal cycle of DMS, such as solar radiation dose (SRD), may not induce the long-term change of DMS (Vallina et al., 2007b). By contrast, the minor factors for DMS seasonal variation may be essential to the DMS change under global warming.

In recent years, the application of data-driven approaches like machine learning to Earth system science has drawn more and more attention. Compared with conventional approaches and process models, machine learning explores larger function space and captures more hidden information from large amounts of datasets, hence it often provides a better simulation and prediction performance (Bergen et al., 2019; Reichstein et al., 2019; Zheng et al., 2020). A recent study has demonstrated that artificial neural network (ANN) can capture more (~66%) of the raw data variance than multilinear regression (~39%) in producing the global climatology of DMS with monthly temporal resolution (Wang et al., 2020). However, this work is lack of the in-depth exploration of relationships between DMS and environmental variables in different regions. The construction of ANN and other machine learning models do not depend on the understanding of explicit mechanisms. Due to the "*black-box*" nature of these models, the complex relationships between target and predictors are stored in nonobvious form and not directly available (Murdoch et al., 2019). Therefore, machine learning models are generally less robust in physical interpretability than theory-driven models (Hou et al., 2022; Molnar, 2020). However, by integrating with appropriate data mining approaches, machine learning models can also be

interpretable to some extent and the output-input relationships may be extracted indirectly (Murdoch et al., 2019).

Here we established a DMS-simulation model based on Global Surface Seawater DMS (GSSD) database (Kettle et al., 1999), datasets of multiple oceanic variables, and ANN approach. Then we simulated the variation of DMS across global oceans and explored the relationships between DMS and environmental variables in 9 separated oceanic regions through global sensitivity analysis and partial dependence plot. Taking the sixth Coupled Models Intercomparison Project (CMIP6) ensemble as the ANN model inputs, the trends of oceanic DMS concentrations and emissions from present to 2100 were projected and the leading influence factors were identified in combination with a series of sensitivity experiments.

2 Materials and Methods

2.1 ANN Training and Validation

The ANN model incorporated 9 variables as input features, including chlorophyll *a* (Chl *a*), sea surface temperature (SST), MLD, nitrate, phosphate, silicate, dissolved oxygen (DO), downward short-wave radiation (DSWF) and sea surface salinity (SSS). The data sources and relevant information of 9 input variables and DMS are listed in Table 1. The GSSD database contains totally 87,801 DMS measurements obtained from 266 cruises and fixed-site observation campaigns during 11 March 1972 to 27 August 2017 (last access: 1 April 2020). The data match-up, filtration and binning were carefully performed as described in Text S1. After these data preprocessing approaches, a total of 34,118 samples were obtained for the ANN model construction and their spatial distribution is shown in Figure 1a, which covers all major regions of global ocean.

As for the ANN training, the target variable is $\log_{10}$(DMS), and the input variables include $\log_{10}$(Chl *a*), SST, $\log_{10}$(MLD), $\log_{10}$(nitrate), $\log_{10}$(phosphate), $\log_{10}$(silicate), DO, DSWF, and SSS. All variables were standardized before training. We randomly selected 5% of binned samples (n = 1706) to be entirely excluded from training, as a subset for global validation and overfitting test. Then, the remaining samples (n = 32,412) were randomly split into three parts, that is, 70% for training, 15% for validation, and 15% for testing. Our feed-forward back-propagation (BP) neural network contains one hidden layer with 20 nodes, and the training algorithm is the Levenberg-Marquardt algorithm. Mean squared error (MSE) is chosen as the indicator for performance evaluation during training, and the upper limit of the number of iterations in each training session is 1000. The training processes were carried out with Neural Network Toolbox on Matlab R2014b, and the URL link to the training code and obtained ANN model is given in Open Research. We have trained the ANN for 100 times to improve the network generalization and performance (Sigmund et al., 2020) and each training session started independently with a new division of those 32,411 samples. The average output of 100 trained ANNs showed a much higher consistency with target than individual ANN. But as the number of training sessions ($N_{training}$) increases, the simulation performance tends to be stable when $N_{training}$ is larger than 100. Therefore, we used the average output of 100 ANNs as our final model output.

157 We divided the global ocean into 9 regions based on Longhurst's biomes (Longhurst,
158 1998). There are 6 biomes in Longhurst's definition, including Coastal, Polar_N, Polar_S,
159 Westerlies_N, Westerlies_S, and Trades (the .shp file of Longhurst's biomes and provinces was
160 downloaded from https://www.marineregions.org/downloads.php#longhurst). We further divided
161 Westerlies_N into Westerlies_N_Pacific and Westerlies_N_Atlantic, and divided Trades into
162 Trades_Pacific, Trades_Indian, and Trades_Atlantic as shown in Figure 1b. In order to evaluate
163 whether there is a spatial preference of DMS simulation, the comparisons of simulated and
164 observed DMS concentrations in each region were conducted.

165 There may be intrinsic connections between the excluded subset and trained dataset,
166 because the data from the same cruise or fixed-site campaign have significant continuity. To
167 further evaluate the reliability of ANN model, we compared the simulated DMS concentrations
168 with the observational data not archived in GSSD database, which are obtained from 35 cruises
169 in Northeast Pacific, West Pacific and North Atlantic (number of data = 6,478). These data
170 include: (1) off-line sampling and measurement data of 31 cruises of *Line P Program* in
171 Northeast Pacific (9 February 2007 – 26 August 2017, number of data = 177,
172 https://www.waterproperties.ca/linep/index.php), (2) underway measurements during *SONNE*
173 *cruise 202/2 (TRANSBROM)* in West Pacific (Zindler et al., 2013) (9 – 23 October 2009, number
174 of data = 115, https://doi.org/10.1594/PANGAEA.805613), (3) underway measurements during
175 3 cruises of the *North Atlantic Aerosols and Marine Ecosystems Study (NAAMES)* (Behrenfeld et
176 al., 2019; Bell et al., 2021) (11 – 30 November 2015, 14 May – 4 June 2016, 6 – 24 September
177 2017, number of data = 6,186, https://seabass.gsfc.nasa.gov/naames).

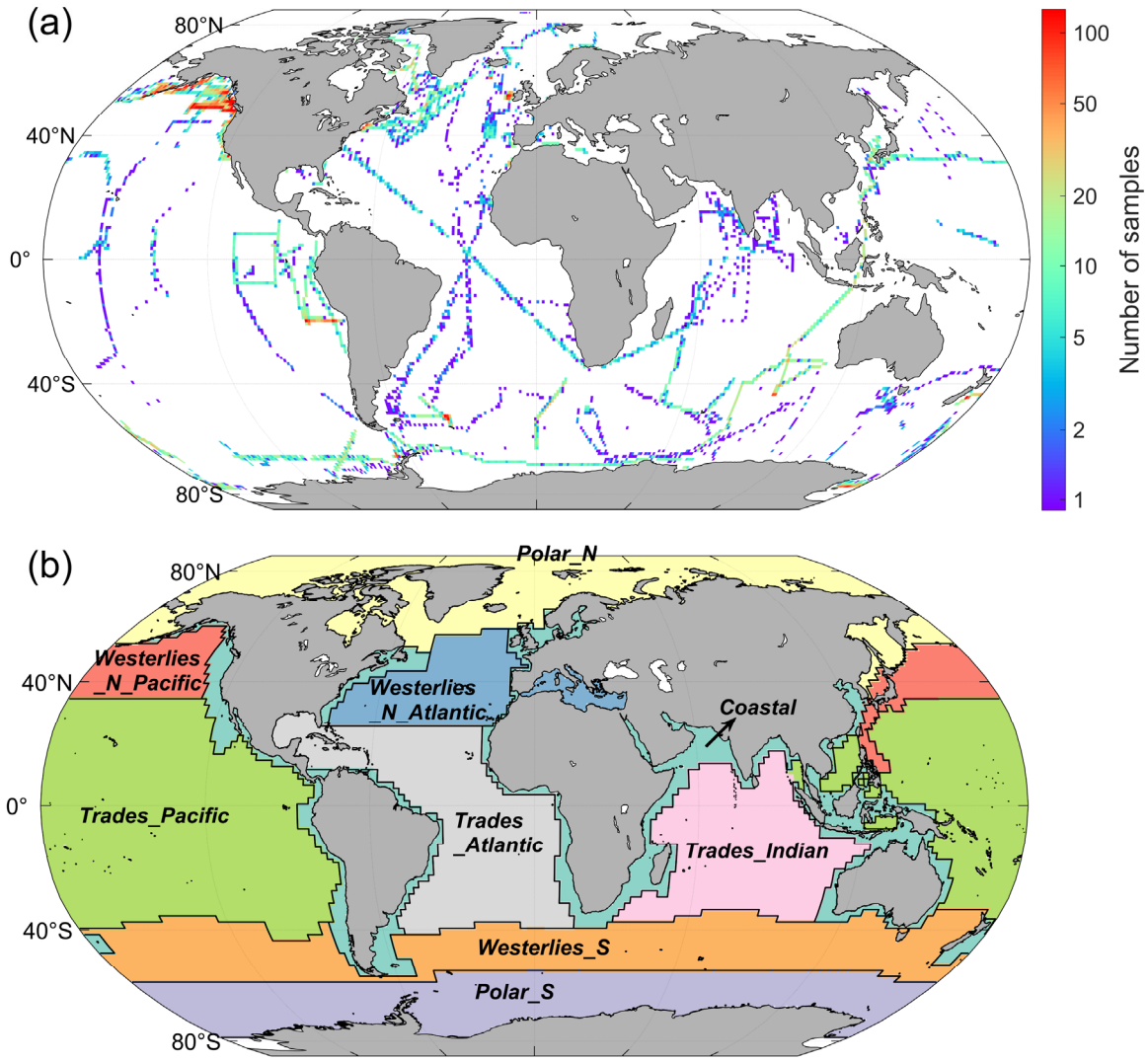

Figure 1. (a) The distribution of 34,118 DMS observational data (after matchup, filtration, and binning) used for constructing the ANN model. The grid size is 1°×1°. (b) Nine oceanic regions separated on the basis of Longhurst's biomes.

Table 1.

The Data Sources and Related Information of Variables Used for Developing the ANN Model, DMS Simulation, and Flux Calculation

Variable	Data source	URL	Temporal resolution	Temporal coverage	Spatial grid
DMS	GSSD database	https://saga.pmel.noaa.gov/dms/	-	Mar. 1972 – Aug. 2017	-
Chl *a*	GSSD database	https://saga.pmel.noaa.gov/dms/	-	Oct. 1980 – Aug. 2017	-

	SeaWiFS	https://oceandata.sci.gsfc.nasa.gov/	Daily, 8-day, monthly	Sep. 1997 - Dec. 2011	0.083°×0.083°
	Aqua-MODIS			Jul. 2002 - present	
SST	NOAA OI SST V2	https://psl.noaa.gov/data/gridded/data.noaa.oisst.v2.highres.html	Daily	Sep. 1981 - present	0.25°×0.25°
MLD	NASA ECCO V4r4	https://data.nas.nasa.gov/ecco/data.php?dir=/eccodata/llc_90/ECCOv4/Release4	Daily	Jan. 1992 - Dec. 2017	LLC90
DSWF					
SSS					
Nitrate	WOA18	https://www.nodc.noaa.gov/OC5/woa18/woa18data.html	Monthly climatology	-	1°×1°
Phosphate					
Silicate					
DO					
WS	NASA ECCO V4r4	https://data.nas.nasa.gov/ecco/data.php?dir=/eccodata/llc_90/ECCOv4/Release4	Daily	Jan. 1992 - Dec. 2017	LLC90
SI	NOAA OI SST V2	https://psl.noaa.gov/data/gridded/data.noaa.oisst.v2.highres.html	Daily	Sep. 1981 - present	0.25°×0.25°

Note. The LLC90 (Lat-Lon-Cap 90) grid is a native grid used for ECCO data, which has 5 faces containing 13 regional tiles covering the global ocean. The spatial resolution of oceanic grids varies from 22 km to 110 km (Forget et al., 2015).

2.2 Simulating Spatiotemporal Patterns of Sea Surface DMS

First, we constructed the daily gridded dataset of input variables with a spatial resolution of 1°×1° during 2005 to 2014 using the data sources listed in Table 1 (except in-situ Chl *a* data). For those datasets with a higher resolution than 1°×1°, values in each 1°×1° grid were averaged. As for satellite Chl *a* data, the priority level was the same as mentioned in Text S1, and SeaWiFS and Aqua-MODIS datasets were combined. As for nutrients and DO, only monthly climatology was provided in WOA18 and the same value was used for all the days of each month. Hence, these variables lack information on inter-annual and day-to-day variations, but the spatial and monthly variations are well captured. After obtaining the input dataset, the spatiotemporal distribution of sea surface DMS concentrations was simulated using the ANN model. Then the sea-to-air fluxes of DMS were calculated as the products of DMS concentrations and total transfer velocities (Kt). In brief, we adopted the bubble scheme (Woolf, 1997) to calculate the water-side transfer velocity (k_w), and the parameterization schemes proposed by Johnson (2010)

to calculate the air-side transfer velocity (k_a) and Henry's law constant (H). The inhibitory effect of sea-ice cover on gas transfer was considered. More detailed information is described in Text S2. The implementation of above approaches to calculate DMS fluxes follows Galí et al. (2019).

2.3 Global Sensitivity Analysis and Partial Dependence Plot

ANN is conventionally seen as a *"black box"* that there is no clear functional relationship between the output and input variables. In order to demystify this *"black box"*, we used global sensitivity analysis (GSA) and partial dependence plot (PDP) to reveal the dominant variables associated with DMS spatiotemporal varaibility and how DMS changes with the change of each variable in different oceanic regions. When exploring the relative importance of one variable, GSA considers the full-space variabilities of all variables simultaneously, rather than hold other variables at certain values for local sensitivity analysis (LSA) which only captures a small portion of the input variability (Wagener and Pianosi, 2019). Therefore, GSA can provide more rigorous results than LSA. Here we applied a variance-based GSA by calculating first-order Sobol′ indices using quasi-Monte Carlo approach (Sobol′, 2001; Sobol′ and Myshetskaya, 2008). The indices in each oceanic region were calculated independently based on the same unified ANN model. This method has been widely used to explore which input mostly influence the model predictions in the field of environmental sciences (Girard et al., 2016; Sigmund et al., 2020; Wagener and Pianosi, 2019). As for PDP, it graphically illustrates the marginal effect of an input variable on the model output, which can be interpreted as the response of output to the change of this input (Haaf et al., 2021; Molnar, 2020; Qin et al., 2022). PDP looks at the input variable of interest across a specified range. At each value of this variable, the output values for all input samples are simulated and then averaged. The detailed calculation processes are provided in Text S3.

2.4 DMS Projection Based on CMIP6 Ensemble

The future (2015–2100) changes of sea surface DMS concentrations and sea-to-air fluxes are projected by applying our ANN model and the ensemble of 11 earth system models in CMIP6 including ACCESS-ESM1-5, BCC-CSM2-MR, CanESM5, CESM2-WACCM, GFDL-ESM4, INM-CM5-0, IPSL-CM6A-LR, MIROC6, MPI-ESM1-2-HR, MRI-ESM2-0 and NorESM2-MM. The projection was subjected into two Shared Socioeconomic Pathway scenarios SSP2-4.5 and SSP5-8.5 (with radiative forcing approaching 4.5 and 8.5 W m^{-2} in 2100, respectively). The sea surface DMS concentrations and fluxes during 2005–2014 are also simulated using the Historical scenario outputs of same CMIP6 models. All model datasets were downloaded from https://esgf-node.llnl.gov/search/cmip6/ (last access: 23 November 2020). The data availability of involved variables for each model is listed in Table S2 and the model selection for Chl *a* and three nutrients are discussed in Text S4. Thresholds were set for some variables as shown in Table S3, while values outside the range were excluded. Then the data of all selected models for each variable were averaged and used as the model inputs to simulate DMS concentrations. Same treatments were applied for near-surface wind speed and sea-ice cover engaged in flux calculation. As for those variables need to be log transformed, the transformation was conducted before the averaging. The time resolution of all datasets was one month, and the spatial grids were unified to 1°×1°.

2.5 Sensitivity Experiments

In order to infer the dominant factors accounting for the projected future change of DMS under global warming, the following sensitivity experiments were designed to isolate the effect of each variable. First, the abovementioned DMS projection with all input variables changing with time was set as the Reference Experiment. Then, we set an experiment for each variable (Variable Experiment) to exam DMS sensitivity to the variable's long-term change. Taking SST Experiment as an example, the SST input was fixed to the values in 2014, while all other input variables still change year by year. If the simulated DMS change (between 2091–2100 and 2005–2014) of SST Experiment was lower (higher) than that of Reference Experiment, it would suggest that the change of SST made a positive (negative) effect on DMS during the simulation period. The difference of DMS changes between Reference Experiment and each Variable Experiment represented the effect intensity of each variable which was used to identify dominant negative and positive factors.

3 Results and Discussion

3.1 Simulation of Ocean Surface DMS by Machine Learning

As shown in Figure 2a, the newly-developed ANN model captures a substantial part of data variance globally ($\log_{10}$ space $R^2 = 0.624$ and RMSE = 0.267). The simulation perfomance for 5% of dataset not used in training ($R^2 = 0.604$ and RMSE = 0.274) is close to that for trained dataset, suggesting no obvious overfitting. The ANN model exhibits much better performance compared to previous empirical and process-based models ($R^2 = 0.01$~0.14) (Tesdal et al., 2016) as well as a recent algorithm based on satellite data ($R^2 = 0.50$) (Galí et al., 2018). In addition, it also shows good capability of simulation in each of 9 separated oceanic regions without significant spatial preference (Figure 2c, $R^2 = 0.376$~0.694, RMSE = 0.152~0.304).

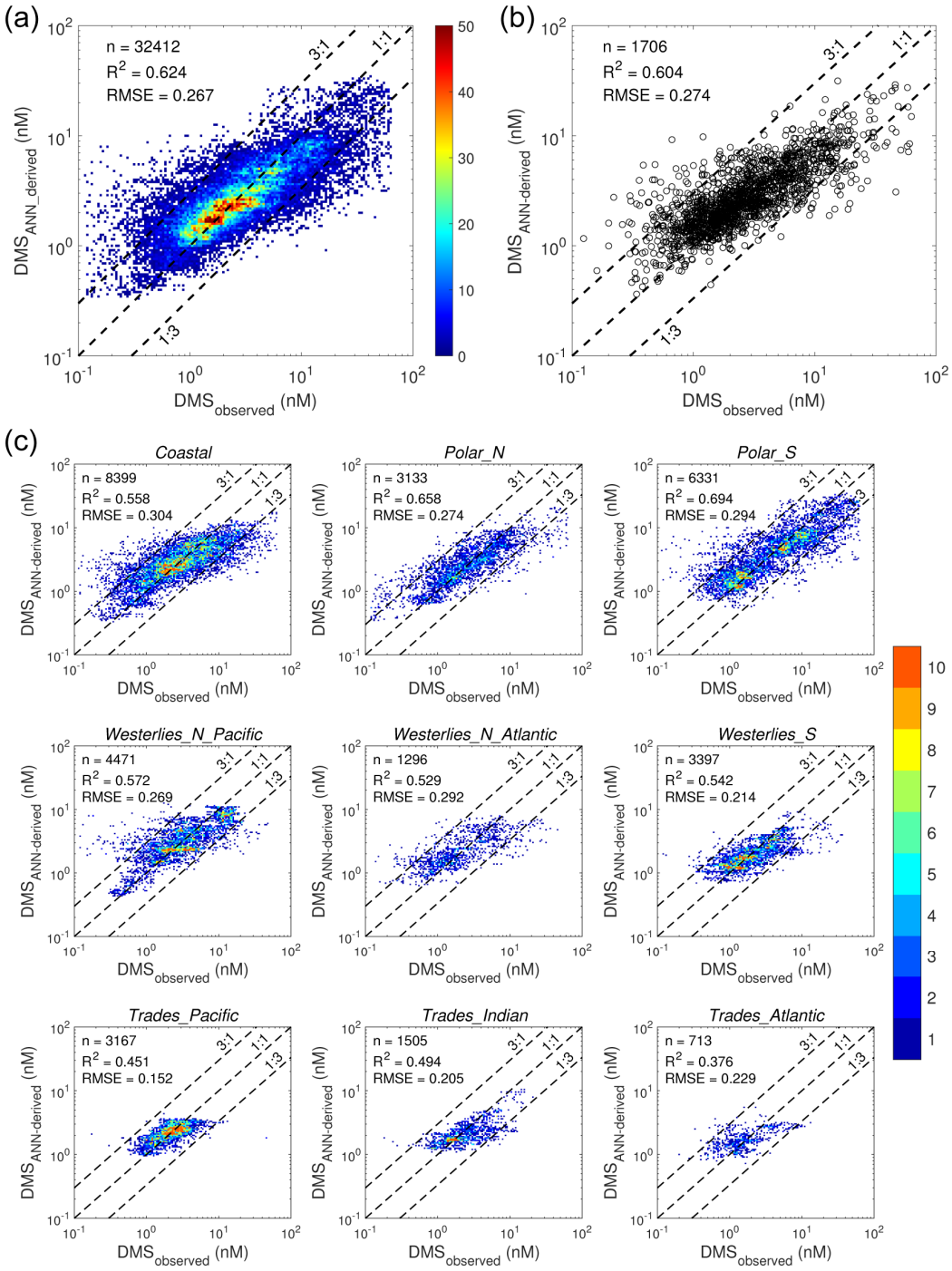

Figure 2. Comparisons between ANN-simulated and observed DMS conentrations in GSSD database. (a) Scatter density for all simulated versus observed DMS concentration data used in ANN training. (b) Comparison between the simulation results and the 5% of GSSD observational data not used for training. (c) Scatter density for simulated versus observed DMS concentration data in each of 9 regionss. The number of data (n), the $\log_{10}$ space R^2 and root mean squared error (RMSE) are also displayed.

The comparisons between observed DMS concentrations not archived in GSSD dataset and ANN simulation results in corresponding 1°×1° grids and dates of samples are shown in Figure 3. As for the *Line P Program*, it should be noted that there are 7 cruises included in GSSD database, but those data were obtained by underway measurements, different from the off-line data used here. Hence, these cruises were retained and marked in Figure 3a but eliminated in subsequent statistical analysis (Figure 3c-3d). It can be seen that the simulation well captures the seasonal variation, which is generally August > June > February. In addition, the simulation can also partially reproduce the changes between different stations, though the performance is not as good as the overall comparison between different cruises. As for underway measurements in West Pacific and North Atlantic, the data were binned by day and 1°×1° grid and then compared with simulated DMS concentrations (Figure 3c). Most of the simulated values are within the range of 1/3 to 3 times of observations. If all above data are binned by each cruise, the simulations will demonstrate higher consistency with observations as shown in Figure 3c (log_{10} space $R^2 = 0.784$, RMSE = 0.227). Therefore, the ANN model has high fidelity in simulating the concentrations of sea surface DMS.

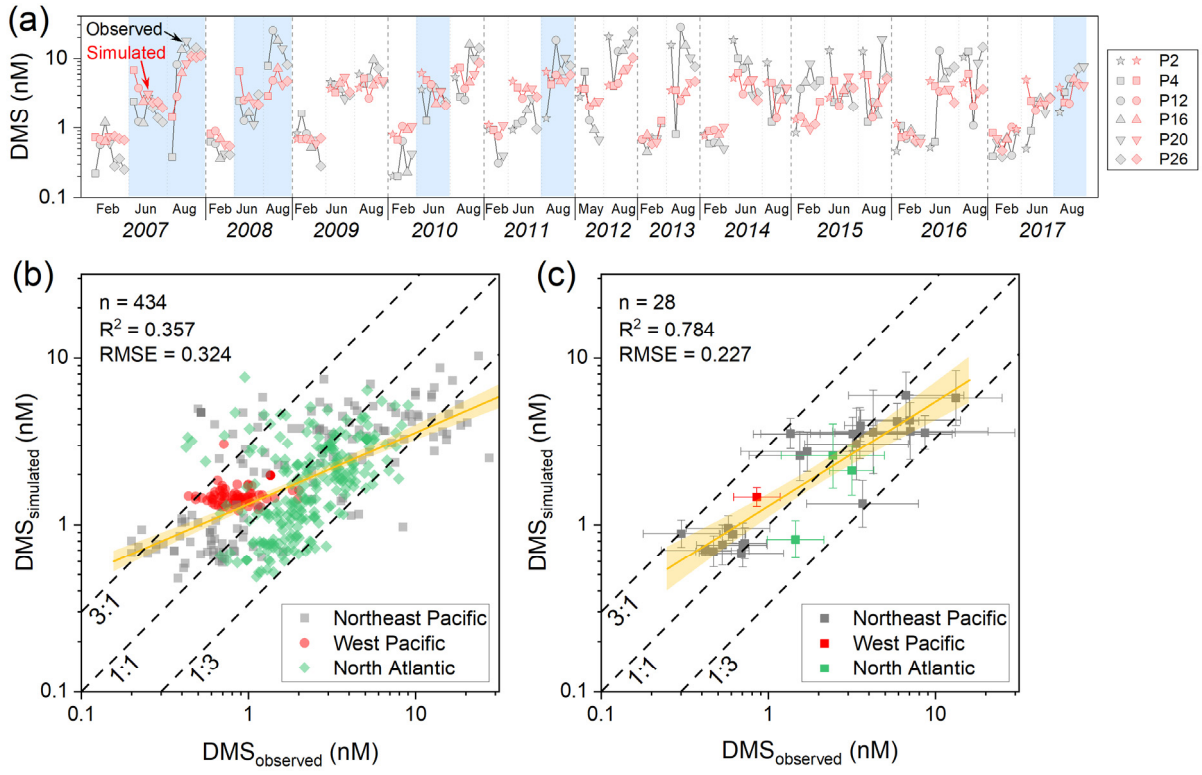

Figure 3. Comparisons between the ANN model simulation results and DMS observational data not archived in GSSD database. (a) Time series of simulation results and DMS observational data obtained from *Line P Program*. The different markers represent different stations of *Line P*. The blue shades cover the data obtained from the cruises included in GSSD database but with a different method. (b) Scatter plot of simulated versus observed DMS concentrations. (c) The same as panel b but for averaged data of each cruise. The yellow lines and shaded bands are

linear fittings and corresponding 95% confidence intervals for $\log_{10}$ space data. The R^2 and RMSE displayed in figure also corresponds to $\log_{10}$ space data.

By applying the ANN model, we obtained a gridded dataset (1°×1°) of daily DMS concentrations in surface ocean and sea-to-air fluxes spanning from 2005 to 2014 (referred to as Z22 dataset). The simulation of atmospheric DMS chemistry by chemical transport models may be effectively improved by taking this dataset as marine DMS emission inventory, due to its higher time resolution than previously used monthly climatology (Hodshire et al., 2019; Novak et al., 2021; Woodhouse et al., 2013). Our estimate of globally area-weighted annual mean concentration of sea surface DMS is 1.86 nM, which is significantly lower than those derived from the SRD-based parameterization (2.71 nM, Vallina and Simó, 2007) and the interpolation-based climatologies (2.43 nM and 2.26 nM from the second version L11 and the third version H22 climatologies, respectively) (Hulswar et al., 2022; Lana et al., 2011), but slightly higher than those estimated by the satellite-based algorithm (1.63 nM, referred to as G18) (Galí et al., 2018) and another ANN model (1.74 nM, referred to as W20) (Wang et al., 2020). High DMS concentrations (> 2.5 nM) occur in the North Pacific and subarctic Atlantic during June-August and at the 40° S of Southern Ocean and near Antarctic continent during December-February (Figure 4a). DMS is also abundant in the eastern Pacific and Benguela upwelling zones, where nutrient-rich deep waters support high primary production. These overall seasonal and geographical distributions generally accord with the previous estimates of global DMS fields, as well as the observed DMS maximum in summer in subtropical to polar open oceans associated with the strongest radiation and water stratification (Simó and Pedrós-Alió, 1999; Vallina and Simó, 2007). Nonetheless, in specific regions our simulation (DMS_{Z22}) may show considerable differences with other DMS estimates (Figure S4-S5). Compared with DMS_{L11}, DMS_{Z22} is significantly lower at high latitudes in summer and in South Indian Ocean and Southwest Pacific Ocean during December to February (Figure S4a). As an update of L11, DMS_{H22} shows much less divergence with DMS_{Z22} in northern high latitudes, South Indian Ocean and Southwest Pacific Ocean, but its summertime concentrations around the Antarctic are much higher than DMS_{Z22} (Figure S4b). DMS_{G18} generally shows milder spatial variation in open oceans and lower values (especially in North Pacific and coastal Antarctic during summer) than DMS_{Z22} (Figure S4c). DMS_{W20} exhibits the highest consistency with DMS_{Z22} in spatiotemporal distribution patterns among the four previous estimates. But there is a significant difference that DMS_{Z22} is generally higher in the region of ~40° S and 0–120° W, and forms a complete annular high-DMS area at 40° S in austral summer (Figure S4d and Figure 4a).

The spatial and seasonal patterns of DMS flux follow its concentration variability with the exception of polar regions where sea-ice cover may prevent the gas transfer to the atmosphere (Figure S7). We obtain highly consistent distributions (Fig. 4b and Figure S6-S7) and values (global mean DMS concentration of 1.88 nM and emission of 19.2 Tg S yr^{-1}) when substituting model inputs by Historical-scenario datasets of CMIP6, suggesting that CMIP6 datasets could be used to project the long-term DMS trend through the ANN model.

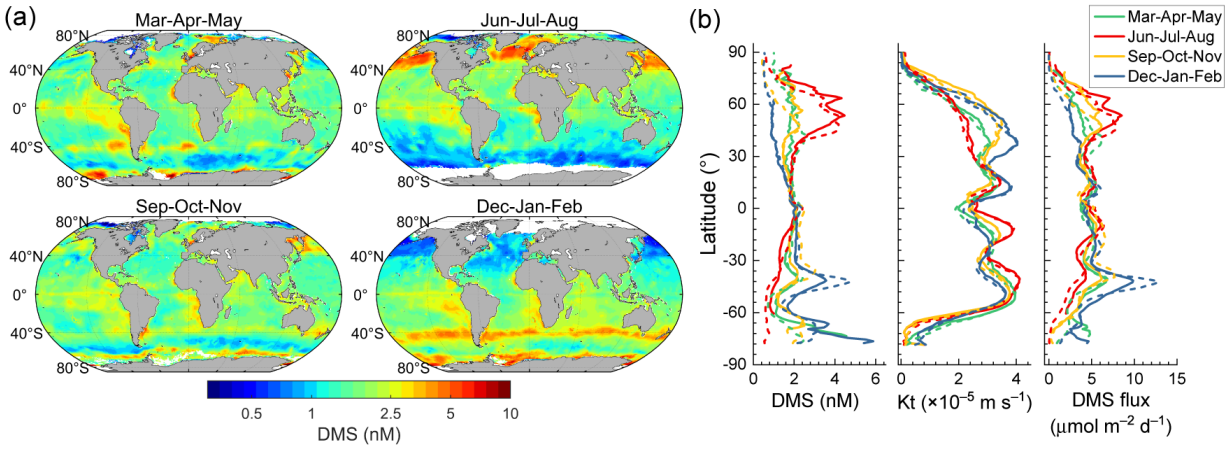

Figure 4. Seasonal distribution of simulated DMS concentrations in the global ocean surface during 2005–2014. (a) Simulated seasonal climatology of global sea surface DMS concentrations during 2005 to 2014 on the basis of the same input datasets as training. (b) The latitudinal distributions of simulated DMS concentration, transfer velocity, and sea-to-air flux in different seasons during 2005 to 2014. The solid and dashed lines correspond to the simulations on the basis of the same input datasets as training and CMIP6 datasets, respectively.

3.2 Relationships between DMS and Environmental Factors

By applying GSA and PDP (see Methods and Text S3), we were able to identify the main environmental factors related with the DMS variability and illustrate the relationship between DMS concentration and each factor in different oceanic regions. For coastal region, the most important factor is Chl *a* (Figure 5), which shows a monotonically positive relationship with DMS (Figure 6), mainly attributed to stronger biogenic sulfur producing with higher phytoplankton biomass. In the Arctic region (Polar_N), the top two controlling factors are SSS and Chl *a* (Figure 5), and they both exhibit positive relationships with DMS (Figure 6). In this region, high SSS is generally accompanied with the inflow of more saline, warmer and nutrient-rich Atlantic water mass (the so-called "Atlantification") (Figure S8), where high abundances of *Phaeocystis pouchetii* were generally found (Schoemann et al., 2005; Vogt et al., 2012). In addition, both seasonal and decadal observations showed that enhanced Atlantification led to an increase in the summertime proportion of *Phaeocystis pouchetii* and decrease of diatoms (Nöthig et al., 2015; Orkney et al., 2020; Reigstad et al., 2002). *Phaeocystis* is likely one of major contributors to dimethylated sulfur compounds at high latitudes (Galí et al., 2021). Therefore, the close link between major DMSP-producing phytoplankton and saline Atlantic waters may partly explain why the SSS is a key influencing factor of the spatiotemporal variations of DMS in the Arctic region. It should be noted that salinity change and water stratification caused by sea-ice melt may also affect phytoplankton biomass and community structure (Ardyna and Arrigo, 2020; Galí et al., 2021), but the specific influence of sea-ice melt on DMS remains to be studied. Our results show that the coastal and Arctic regions belong to *bloom-forced regime* for DMS cycling, which is consistent with previous statements (Toole and Siegel, 2004). The importance of Chl *a* to DMS in the Arctic can also explain why good correlation between DMS and net primary

productivity occurred therein, which is a prerequisite for using ice-core MSA concentrations to reconstruct multi-century change of subarctic oceanic productivity (Osman et al., 2019). Nonetheless, Chl *a* is not a dominant factor in mid-latitude and tropical open oceans (Longhurst's Westerlies and Trades biomes (Longhurst, 1998)), agreeing with the mismatch between annual cycles of DMS and Chl *a*, i.e. "DMS summer paradox" (Galí and Simó, 2015; Simó and Pedrós-Alió, 1999), which corresponds to the *stress-forced regime*. Instead, DSWF and MLD generally rank among the top three key factors, and DMS increases with the increase of DSWF and the decrease of MLD when MLD < 140 m (Figure 5-6), consistent with the significant role of SRD in controlling the DMS variation in upper mixed layer (Vallina and Simó, 2007; Vallina et al., 2007a). The consistency between former knowledge and our results of DMS controls can well prove that the combination of machine learning, GSA, and PDP approaches is a viable way to explore the complex relationships between DMS and various environmental factors.

Macronutrients are also important factors in mid-latitude and tropical oceans, such as nitrate in Westerlies_N_Pacific and Westerlies_S; and phosphate in Westerlies_N_Atlantic, Westerlies_S, Trades_Pacific, and Trades_Atlantic (Figure 5). Nutrients demonstrate negative and positive effects on DMS at their low and high concentrations respectively (Figure 6), with the turning points of 0.030–0.122 μmol kg^{-1} nitrate and 0.025–0.032 μmol kg^{-1} phosphate in three Trades regions and 0.62–14.2 μmol kg^{-1} nitrate and 0.021–0.11 μmol kg^{-1} phosphate in Westerlies. High nutrients normally supply flourishing phytoplankton biomass leading to a high production of biogenic sulfur. However, in extremely nutrient-depleted regime, the biosynthesis of DMSP and its cleavage into DMS and acrylate may also be enhanced, which act as a substitute of nitrogen-containing osmolytes like glycine betaine (Stefels, 2000), dissipate the excess reduced sulfur and carbon under unbalanced growth (Stefels, 2000; Stefels et al., 2007), or establish an anti-oxidation system to eliminate reactive oxygen species (ROS) (Sunda et al., 2002; Sunda et al., 2007). Moreover, nitrate may also enhance the DMS removal by photolysis (Bouillon and Miller, 2005; Toole et al., 2004), although it usually plays a secondary role compared to chromophoric dissolved organic matter (CDOM) (Galí et al., 2016). This mechanism may be particularly important in the Westerlies_S where nitrate concentrations are high and show mainly a negative relationship with DMS (Figure 6). As diatoms are generally low-DMSP producers (Keller et al., 1989), the importance of silicate to DMS is only found in Weterlies_S where the dominant phytoplankton group varies clearly between diatoms and other species around the year (Alvain et al., 2008). In this region, silicate ranks the second important factor and shows an inverse relationship with DMS when its concentration is within the range of 0.16–22.7 μmol kg^{-1}.

Sea surface temperature is the most important factor in southern polar region (Polar_S) (Figure 5), and a sharp increasing trend of DMS is found with the decreasing SST from 4.7 °C (Figure 6). The Southern Ocean is the largest high-nutrient low-chlorophyll (HNLC) region with the primary productivity limited by iron. In the Antarctic shelf, iron is much more abundant supporting higher seasonal productivity compared to off-shelf area (Charette et al., 2013; Tagliabue et al., 2012), although the SST of shelf is generally lower (Figure S9). In addition, *Phaeocystis antarctica* are dominant DMSP producers in Polar_S (DiTullio et al., 2000; Wang et al., 2015; Wang et al., 2018), which well adapt to low temperature (Schoemann et al., 2005) and often bloom with sea ice melt in the Antarctic shelf and the Ross Sea (DiTullio et al., 2000), where our simulated DMS concentrations are also relatively high (Figure S9). Additionally,

culture experiments have corroborated that low temperature can stimulate the DMSP production by *Phaeocystis antarctica* and subsequent DMS release (Baumann et al., 1994; Wittek et al., 2020) since DMSP may act as cryoprotectant (Stefels, 2000; Stefels et al., 2007). Therefore, the spatial overlap of high biomass of DMSP producer with low SST and the cryoprotective effect of DMSP at cold temperature may both contribute to the negative relationship between DMS and SST in the Polar_S. In Trades biomes, SST is also an important factor showing negative relationship with DMS, but the physiological mechanism may be different from that in Polar_S. Together with Westerlies biomes and Polar_N, it seems that there is an optimum SST between 10–20 °C at which the relationship between DMS and SST shifts from positive to negative (Figure 6). Similar relationships have been reported between surface Chl *a* concentrations and SST with the turning point at around 14 °C (7.18–21.06 °C), attributed to the combination of a positive effect of warming on phytoplankton growth rate and its negative effect on nutrients supply to more stratified upper layer (Feng et al., 2021). Although Chl *a* concentration has little contribution to DMS seasonal dynamics in tropical and temperate open oceans, the long-term DMS evolution driven by the change of phytoplankton biomass and community composition caused by the combined effects of SST and nutrients is possible.

It is noteworthy that only the first-order Sobol′ indices are calculated here, which means our GSA only reveals the "main effect" of individual variable. Further studies, like the derivation of second- or third-order Sobol′ indices, need to be conducted in the future to better dissect the controlling factors, their synergistic effects, and underlying biogeochemical processes. Moreover, the PDP is a global method (Molnar, 2020), which presents the average marginal effect of a certain factor on DMS concentration across all seasons and the entire space. Hence, the PDP-revealed relationship between DMS and this factor cannot be interpreted as a universal law that holds in every place or every season.

437

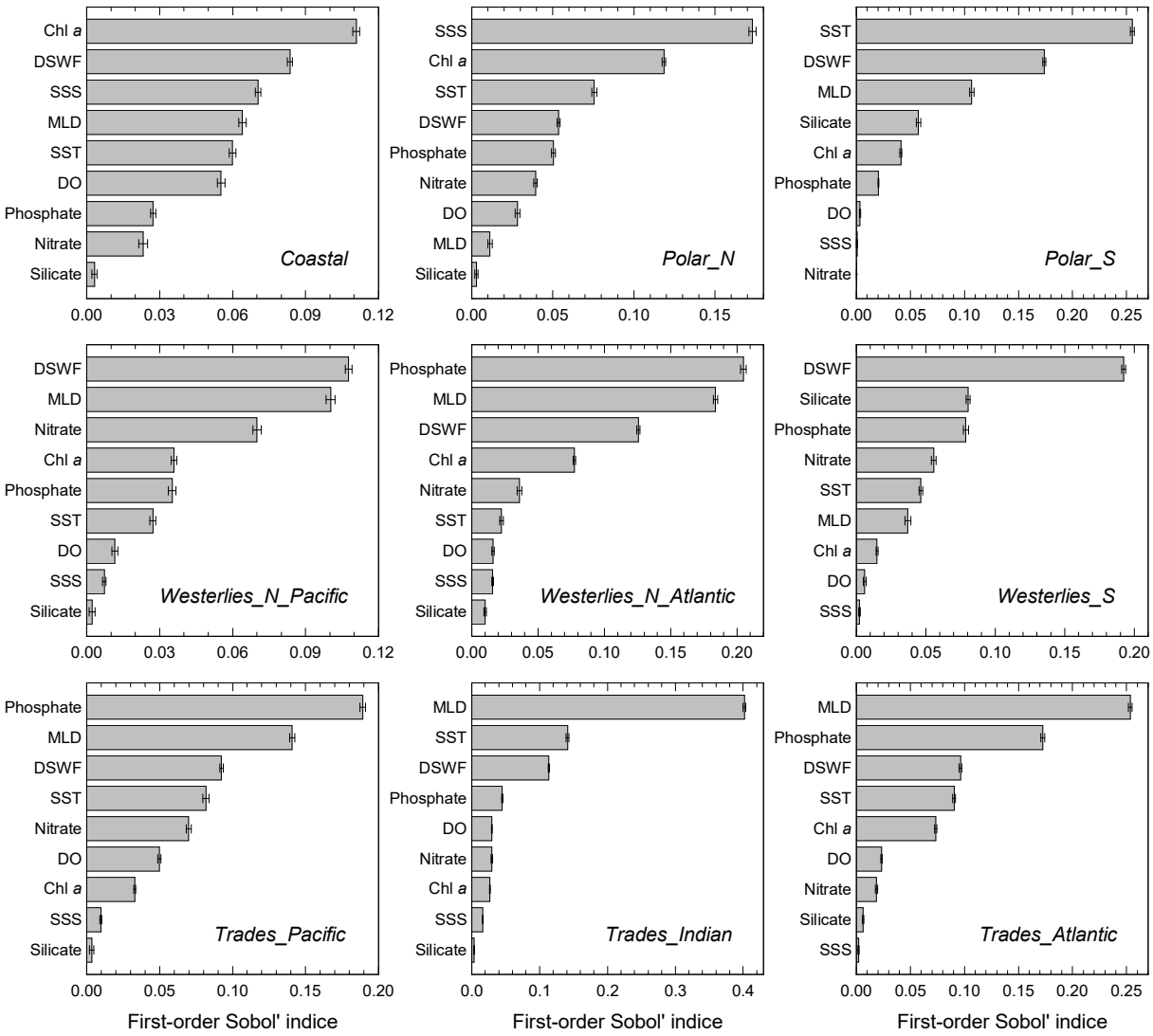

438

439 **Figure 5.** The first-order Sobol′ indices of input variables for different oceanic regions. A larger
440 value indicates relatively higher importance of this variable. The error bars represent the standard
441 deviations of 20 times calculation.

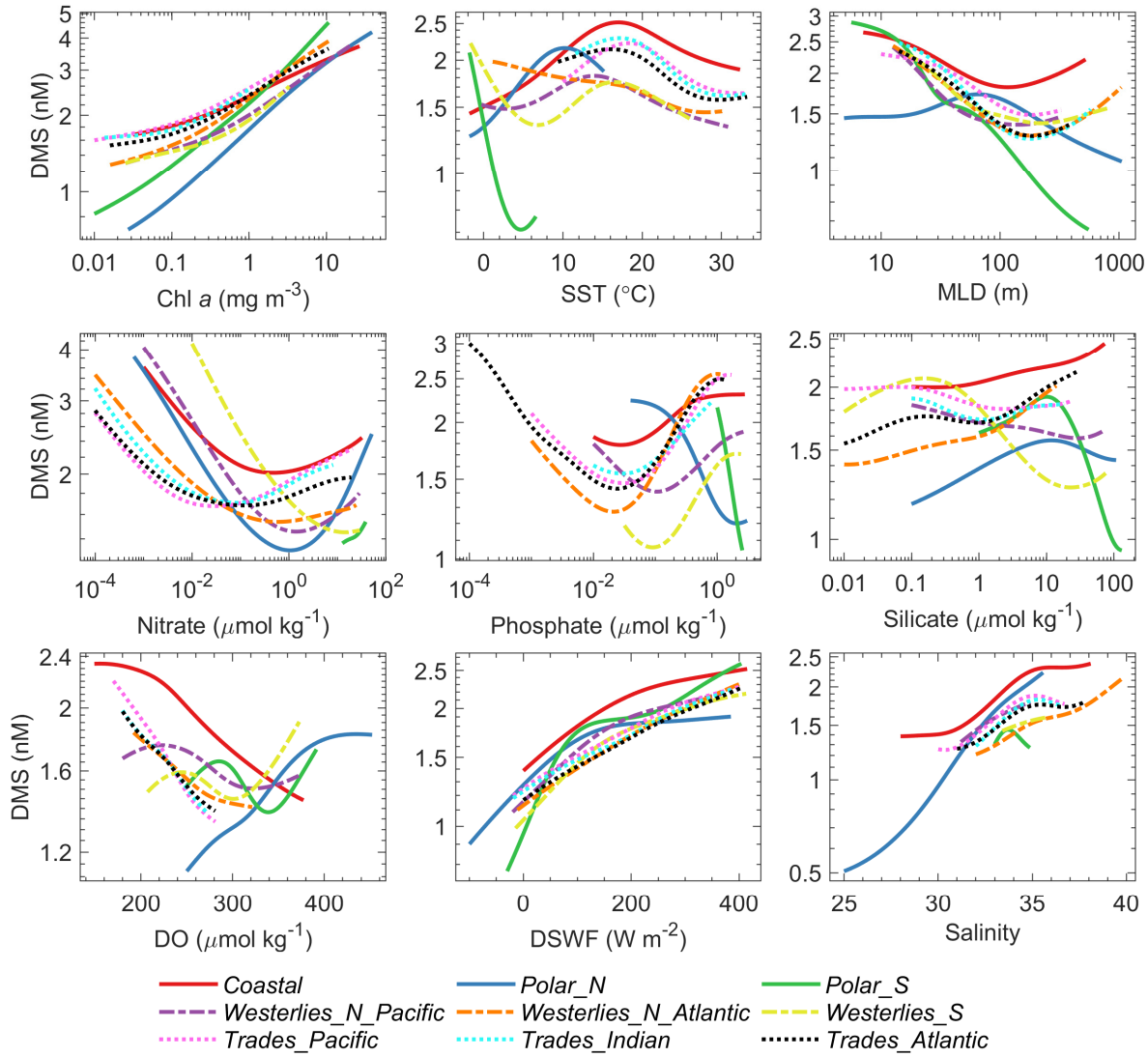

Figure 6. Partial dependence plots for each variable in different regions.

3.3 DMS Change under Global Warming and Influencing Factors

The future changes of sea surface DMS (2015-2100) under SSP2-4.5 and SSP5-8.5 scenarios were simulated by the ANN model using CMIP6 ensemble and their dominant influencing factors were untangled. The global mean concentrations of oceanic DMS decline to 1.78 and 1.75 nM in 2091-2100 (decrease by 5.1% and 7.0% compared to 1.88 nM during 2005-2014) under SSP2-4.5 and SSP5-8.5, respectively. The spatial pattern of the DMS change matches well between these two scenarios, while the degree of change under SSP5-8.5 is relatively more significant (Figure 7a and Figure S10a). Above half (63.0–64.2%) of global oceans exhibit a decreasing trend ($P < 0.05$ for linear regression), especially in the vast tropical

and subtropical Pacific oceans and the subpolar gyre of North Atlantic. The increasing trend will take place mainly in the Southern Ocean, Antarctic shelves, North Pacific, the subtropical gyre of North Atlantic and part of the Arctic and Indian Oceans, which totally occupy 24.6–27.0% of global oceanic area.

The decreasing trend of DMS concentration in tropical and subtropical Pacific oceans is predominantly related with the phosphate reduction and SST increase (Figure 8-9 and Figure S13-S15). The phosphate concentration and SST in this region are mostly above the turning points revealed by PDPs and demonstrate positive and negative relationships with DMS respectively, hence their future changes will both result in the decline of DMS (Figure 9a). Additionally, the overall phytoplankton biomass may decline in the warmer and nutrient-deficient ocean evidenced by both long-term observations (Boyce et al., 2010) and numerical modeling (Kwiatkowski et al., 2019), whereas picophytoplankton (cyanobacteria *Prochlorococcus* and *Synechococcus* and picoeukaryotes) are suggested to be promoted (Flombaum et al., 2013; Flombaum et al., 2020). Therefore, picophytoplankton may outcompete high-DMSP producers (such as Haptophyceae and Dinophyceae) in the mid- or low-latitudes, and such community shifts are likely to be one mechanism for DMS decrease. In addition to Pacific, the negative effects of these two factors on DMS in low- to mid-latitude Atlantic and Indian Oceans are also universal and significant (Figure 9c and Figure S14-S15). In contrast, the phosphate reduction and SST rise in the Arctic Ocean may lead to DMS increase because their values are below the turning points (Figure 9a). But in high-latitude Southern Ocean near the Antarctic (> 55° S, Polar_S), the increasing SST will make a negative effect probably due to the cryoprotective function of DMSP and its high production in extremely cold waters as shown in PDP (Figure 6). Therefore, the same future trend of a specific factor may cause totally different effects on DMS changes in different regions, which is highly dependent on the background conditions. In Polar_S, the positive effect of silicate reduction will surpass the abovementioned negative effect of SST and lead to a net DMS increase, which may be attributed to the species succession from diatom to high-DMSP producers such as *Phaeocystis antarctica* (Cameron-Smith et al., 2011; Wang et al., 2018) (Figure 8-9 and Figure S13-S15).

The poleward shifts of oceanic physical and ecological zones generally occur under global warming (Barton et al., 2016; Yang et al., 2020). Similarly, the high-DMS regions in the North Pacific and Southern Ocean (Westerlies_S) also move to higher latitudes (e.g. the DMS concentration in the Southern Ocean peaks at 43°–44° S during 2091–2100 under SSP5-8.5 compared with 40°–41° S during 2005–2014, Figure 7a) mainly explained by the SST rise and increased stratification (Figure 9). This is particularly important owing to the critical role of marine biogenic sulfate in cloud formation over the lower Southern Ocean latitudes (35°–45° S) (McCoy et al., 2015), and change of cloud cover pattern may influence the regional atmospheric circulation and albedo. A recent study based on global observations from 1970 to 2018 showed that the summertime mixed layer was deepening concurrently with the increase of upper ocean stratification in response to global warming (Sallee et al., 2021). However, current CMIP6 models do not capture these trends, which may result in considerable uncertainties for our projection and calls for the model improvement regarding this issue in next CMIP generation.

Given the positive relationship between DMS and SSS (Figure 6), the dramatic decrease of SSS in the North Atlantic subpolar gyre (Figure 8 and Figure S13) associated with the strengthening of global water cycle (Durack et al., 2012), the freshwater influx from the Arctic

Ocean and the Greenland (Huang et al., 2014), and the weakening of Atlantic meridional overturning circulation (AMOC) (Zhu and Liu, 2020) is found to be the dominant factor accounting for DMS decline (Figure 9c and Figure S14b). It should be noted the decline in DO will cause universal positive effect on DMS in most of low- to mid-latitude oceans, but its effect generally cannot outcompete the negative effects of SST and phosphate (Figure 9b-c an Figure S14). In addition, the dominant factor controlling the current spatial variation or seasonal cycle of DMS in certain oceanic regions may not induce the long-term DMS change. For example, DSWF is one of the most important factors controlling the spatiotemporal pattern of DMS (Figure 5), but it makes nearly no effect on DMS change from 2005 to 2100 (Figure 9b and Figure S14b) because its annual values basically remain stable during the whole period (Figure 8 and Figure S11).

Due to the ubiquitous warming of surface water, the total transfer velocity (Kt) of DMS generally increase in most of global ocean (Figure 7 and Figure S10). As a result, the decline of global oceanic DMS emission (1.8% for SSP5-8.5) will be much smaller than the decrease (7.0%) of its concentration, from 19.15 Tg S yr^{-1} in 2005–2014 to 18.82 Tg S yr^{-1} in 2091–2100 (Table S4). The change of DMS fluxes coincide spatially with its concentrations in mid- and low-latitude oceans. But in the Arctic Ocean, due to the striking loss of summertime sea-ice cover (Figure 10a), the Kt and sea-to-air flux of DMS exhibit extensive and significant rise (Figure 7b-f). Specifically, the summertime DMS emission will increase by approximately 73% from 42.4 Gg S yr^{-1} (2015) to 73.3 Gg S yr^{-1} (2100) under SSP5-8.5 scenario in the >70° N Arctic (Figure 10c), which accords with the decadal increase in Arctic DMS emission between 1998 to 2016 reported in a recent study (Galí et al., 2019). This result highlights the importance of sea-ice retreat to biogenic sulfur emission and subsequently aerosol radiative forcing, likely leading to a negative feedback in Arctic climate system, which is warming faster than any other regions (Levasseur, 2013). It should be noted that some previous studies have pointed out the remarkable contribution of bottom-ice DMS production to sea surface DMS concentration and flux to the air in specific months (Hayashida et al., 2020), which is not considered in this study. However, this process is still highly uncertain due to the scarcity of observations, and the ice-to-sea DMS flux is likely to make little impact on the upward trend of sea-to-air DMS emission (Hayashida et al., 2020). As for the Antarctic with latitude larger than 65°, the summertime sea-ice loss is relatively weaker than that in the Arctic and the average DMS concentration presents a slight decrease. Therefore, the increasing proportion of summertime DMS emission is much lower, from 140 Gg S yr^{-1} in 2015 to 169 GgS yr^{-1} in 2074 (21%) and then decrease to 157 GgS yr^{-1} in 2100.

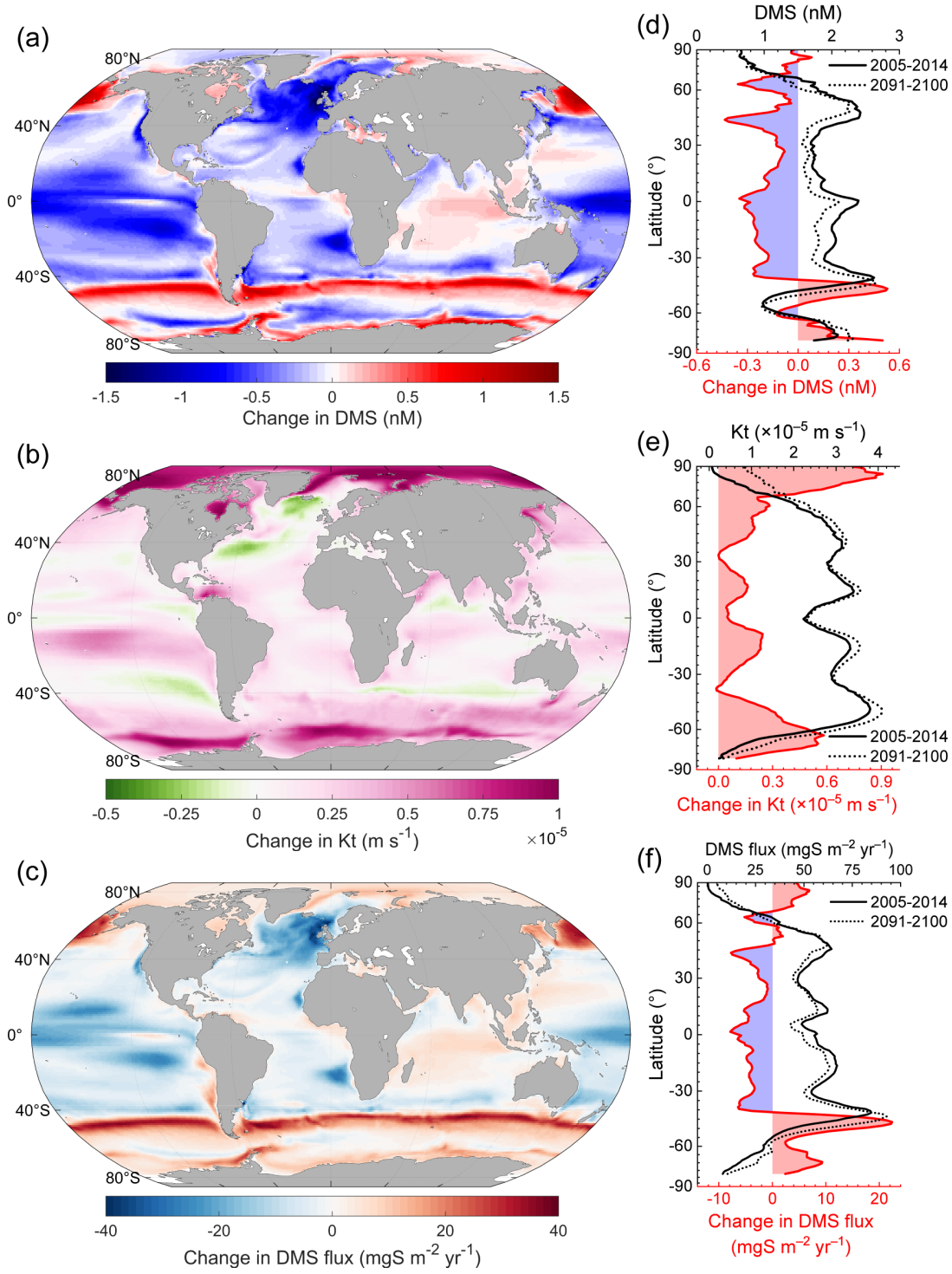

Figure 7. Projected changes in sea surface DMS concentration, transfer velocity (Kt), and sea-to-air flux under SSP5-8.5 scenario. (a-c) Spatial distributions of the future changes (between 2091–2100 and 2005–2014) of (a) DMS concentrations, (b) transfer velocities, and (c) DMS fluxes in the global ocean surface based on CMIP6 datasets. (d-f) Latitudinal distributions of the mean (d) DMS concentrations, (e) transfer velocities, and (f) emission fluxes in the global ocean

surface in 2005–2014 (solid black lines) and 2091–2100 (dash black lines) and the changes between these two periods (red lines with light blue and red shades representing negative and positive changes, respectively).

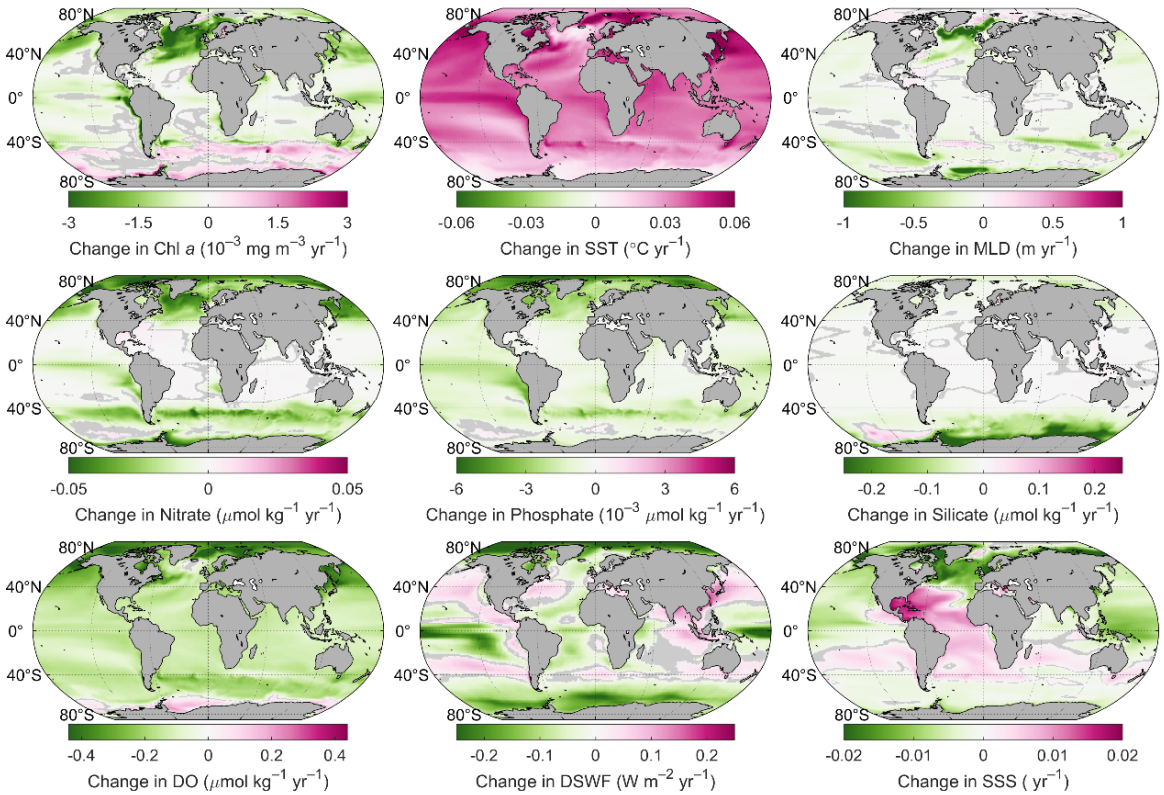

Figure 8. Changing rate of each variable from 2015 to 2100 for SSP5-8.5. The gray area in the ocean represents no significant change (P > 0.05 for linear regression of yearly data).

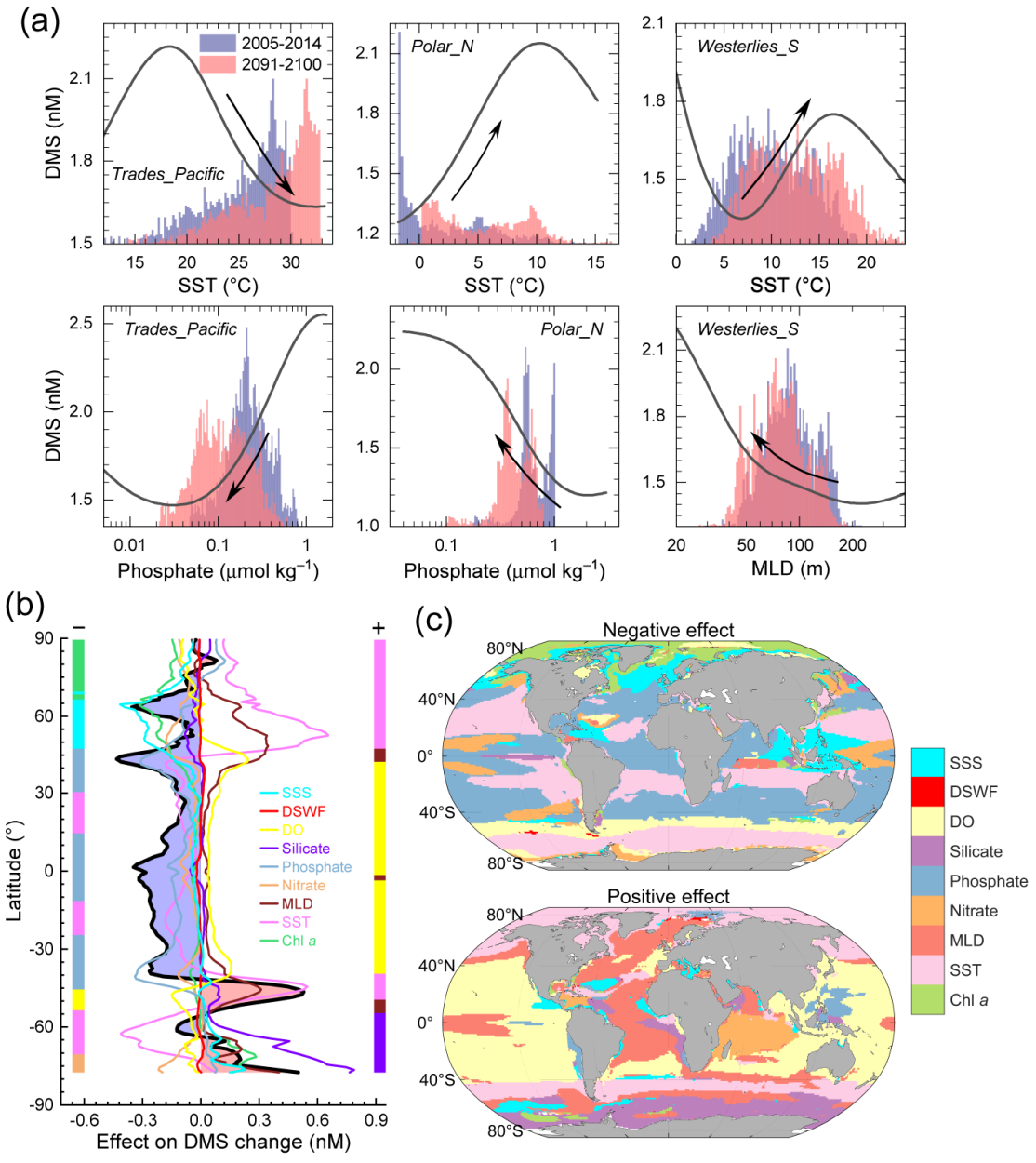

Figure 9. Attribution of the future changes of sea surface DMS concentration under climate warming. (a) Histograms of environmental factors in 2005–2014 and 2091–2100 (SSP5-8.5) as well as partial dependence plots (solid lines) showing how the changes of environmental factors affect DMS concentration in different regions. The illustrated factors include SST and phosphate for Trades_Pacific and Polar_N, and SST and MLD for Westerlies_S. The histograms were plotted on the basis of 5,000 samples by area-weighted random sampling from initial gridded dataset of each region. (b) Latitudinal distribution of the average effect of each factor on DMS future change. The bold black line shows the simulated latitudinal distribution of DMS change between 2091–2100 and 2005–2014. The left and right color bands illustrate dominant negative and positive factors at different latitudes, respectively. The dominant factor refers to the factor

with the largest absolute value of effect on DMS change. (c) Spatial distributions of the dominant negative and positive factors related with the DMS change across global oceans.

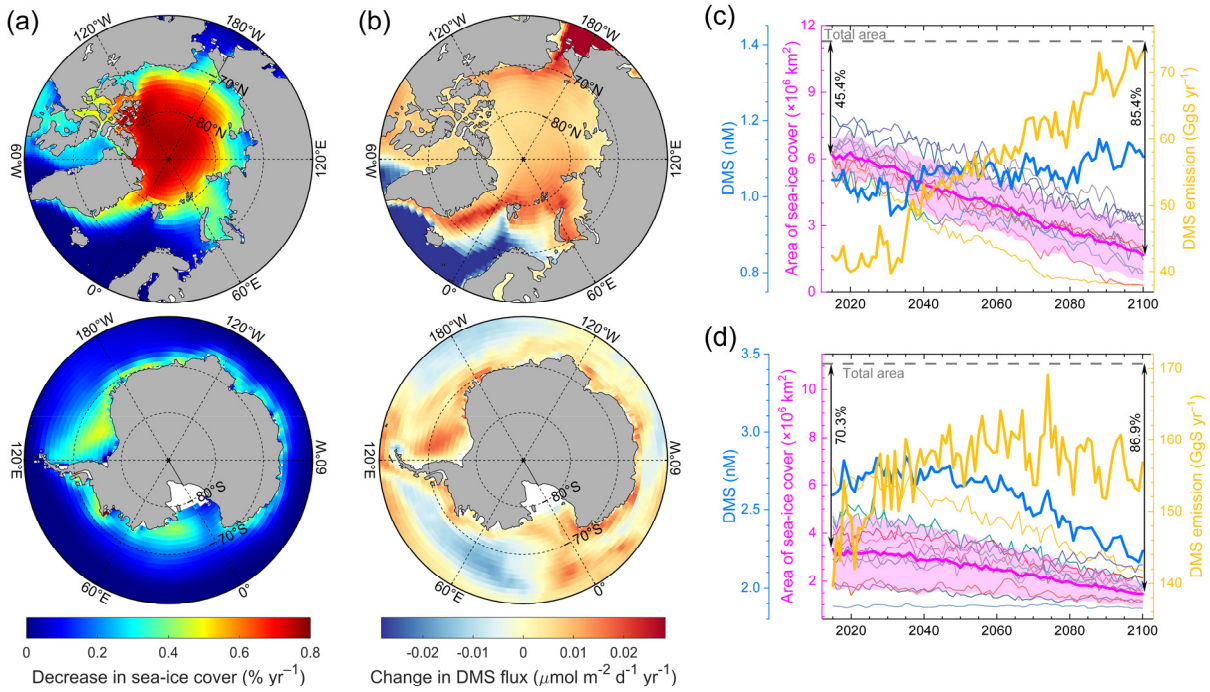

Figure 10. Changes in summertime sea-ice cover and DMS in polar regions during 2015–2100 for SSP5-8.5 scenario. (a) The spatial distributions of absolute decreasing rates of summertime (May–September for the North Pole and December–April for the South Pole when sea-ice cover is low and DMS emission is high in a year) sea-ice covering fraction. (b) The spatial distributions of changing rates of summertime DMS flux. (c-d) The time series of averaged summertime DMS concentration, area of sea-ice cover, and DMS emission for the (c) North pole with latitude larger than 70° and (d) South pole with latitude larger than 65°. The thin lines represent area of sea-ice cover obtained from each of CMIP6 models and the purple thick line and shaded bands represent the average and standard deviation of these models. The proportions of ice-free extent to total area in 2015 and 2100 are presented.

5 Conclusions

Sea surface DMS distribution and its change under global warming have been simulated by characterizing main processes of DMS cycle and/or using empirical parameterization of influencing factors like Chl *a*, MLD, radiation and nutrients (Bock et al., 2021; Cameron-Smith et al., 2011; Gabric et al., 2004; Kloster et al., 2007; Six et al., 2013; Vallina et al., 2007b; Wang et al., 2018). However, distinct ocean environments and complexity of DMS production and cycle lead to striking biases in modeling DMS on a global scale. Data-driven approaches like ANN are a good supplement to conventional process-based (theory-driven) and empirical models.

Overall, the ANN model we developed can well reproduce the variability of sea surface DMS across the global ocean, which provides a foundation for analyzing the relationships between DMS and environmental variables at current situations and for projecting the DMS trends in the future. The simulated global annual average DMS concentration is ~ 1.9 nM and the emission is 19.2 Tg S yr^{-1} during 2005 to 2014. High values generally occur in North Pacific, subarctic Atlantic, the 40° S of Southern Ocean and Antarctic shelves at hemispheric summer. By applying the variance-based GSA and PDP approaches, which factor is the most important to current DMS variability and how these relationships display in nine oceanic regions are systematically investigated. The results show that there are large spatial disparities in dominant influencing factors and the same variable may have reverse effects in different regions. For example, Chl *a* and SSS are the most important factors in Coastal and Polar_N biomes both showing positive relationships with DMS concentrations. In the mid- to low-latitude open oceans, in addition to mixed layer depth and solar radiation, SST and nutrients (mainly phosphate and nitrate) are also important factors. There is probably an optimal SST between 10–20 °C, and the nutrients also exhibit reverse effects on DMS below and above certain turing points. In cold environment Polar_S, SST is the most important factor showing a negative effect.

Using CMIP6 model ensemble as input datasets, the future changes in DMS concentration and flux were projected. For a specific region, the dominant factors accounting for DMS future changes may not coincide with the controlling factors for its current variations. The vast low-latitude Pacific present decreasing trend which is mainly related with phosphate decline and SST rise. The decrease of SSS may induce significant DMS decline in the North Atlantic subpolar gyre. In the North Pacific and Southern Ocean, the warming and increasing stratification may lead to the increase of DMS, and the high-DMS zones exhibit an obvious poleward shift. In general, the global mean concentration of sea surface DMS and global emission of DMS to the atmosphere will both decline slightly in the 21st century, although large spatial heterogeneity exists. These results seem adverse to part of "CLAW hypothesis" which assumed increased emission of oceanic DMS under global warming. But the climatic effect caused by future changes of oceanic DMS relies on further exploration and understanding of atmospheric DMS chemistry and aerosol-cloud-radiation interactions (Hoffmann et al., 2016; Novak et al., 2021; Veres et al., 2020). Nonetheless, the dramatic increase of DMS emission caused by sea-ice loss in the Arctic Ocean in future may lead to a CLAW-like negative feedback. Considering the diverse trends of DMS fluxes in different oceanic regions, the future evolution of marine DMS emission pattern may profoundly affect the regional cloud cover, albedo and atmospheric circulation to some extent.

In this study, we have not incorporated any apriori information into the processes of model construction, relationship exploration and dominant factor identification, but the results seem reasonable and explainable, suggesting the good performance of data-driven techniques in DMS prediction and information mining. However, disadvantages also exist. For example, what we have obtained from GSA, PDP, and sensitivity experiments for future prediction are just statistic results. In other words, what are "interpretable" directly extracted are just the output-input relationships for the ANN model itself, but not explicit causal mechanisms for DMS cycling. The mechanistic interpretations need to incorporate existing knowledge on underlying processes acquired by conventional techniques (e.g., culture experiments and process models). In addition, several studies have pointed out that seawater pH makes a great impact on DMS cycle as well as its response to future climate change (Arnold et al., 2013; Deng et al., 2021; Hopkins

et al., 2010; Six et al., 2013), but pH cannot be taken as a variable in the ANN model to project future DMS changes since future pH values will substantially fall outside its present range used in model construction. Actually, large uncertainties also exist in the previous study by applying the relationships between DMS and pH obtained from a few experiments in small regions to global projection (Six et al., 2013). In the future, the coupling of data-driven and theory-driven models will be more powerful to predict the distribution and untangle controlling factors and processes, with the help of more field observations and culture experiments as well as better mechanism understanding.

Acknowledgments

We greatly thank National Oceanic and Atmospheric Administration's Pacific Marine Environmental Laboratory for maintaining the Global Surface Seawater DMS Database. We acknowledge the World Climate Research Programme's Working Group on Coupled Modelling, which is responsible for CMIP6. We acknowledge Dr. Chenzhao Li for sharing the code of global sensitivity analysis and Dr. Martin Johnson for sharing the code of DMS transfer velocity calculation. We also thank Dr. Rich Pawlowicz for developing and sharing the M_Map toolbox for Matlab (https://www.eoas.ubc.ca/~rich/map.html), which was used in the mapping of this study. We also thank State Environmental Protection Key Laboratory of Land-Sea Integrated Management and Regulating Techniques and Research Station for Wetland Ecosystems of the Yangtze Estuary for support. This work is jointly sponsored by Natural Science Foundation of Shanghai (22ZR1403800), National Key Research and Development Program of China (2016YFA0601304), and National Natural Science Foundation of China (41775145).

Open Research

All data used for ANN model construction and the simulation of DMS during 2005–2014 are publicly available, and their sources are listed in Table 1. DMS data used for evaluating the validity of simulation are available from the *Line P Program* website (https://www.waterproperties.ca/linep/index.php), the PANGAEA web page (https://doi.org/10.1594/PANGAEA.805613), and the NASA's SeaBASS repository (https://seabass.gsfc.nasa.gov/naames). CMIP6 model data are downloaded from the CMIP6 portal https://esgf-node.llnl.gov/search/cmip6/. The ANN model code and the Matlab scripts for data analysis are available from https://github.com/SQZhou95/Sea_surface_DMS_simulation_using_neural_network. All DMS concentration and flux simulation data in this study have been deposited in https://doi.org/10.5281/zenodo.7057825 and can be downloaded publicly.

References

Alcolombri, U., Ben-Dor, S., Feldmesser, E., Levin, Y., Tawfik, D. S., and Vardi, A. (2015), Identification of the algal dimethyl sulfide–releasing enzyme: a missing link in the marine sulfur cycle, *Science*, *348*(6242), 1466-1469.

Alvain, S., Moulin, C., Dandonneau, Y., and Loisel, H. (2008), Seasonal distribution and succession of dominant phytoplankton groups in the global ocean: A satellite view, *Global Biogeochemical Cycles*, *22*(3), GB3001, doi:10.1029/2007gb003154.

Andreae, M. O. (1990), Ocean-Atmosphere Interactions in the Global Biogeochemical Sulfur Cycle, *Marine Chemistry*, *30*(1-3), 1-29, doi:Doi 10.1016/0304-4203(90)90059-L.

Ardyna, M., and Arrigo, K. R. (2020), Phytoplankton dynamics in a changing Arctic Ocean, *Nature Climate Change*, *10*(10), 892-903, doi:10.1038/s41558-020-0905-y.

Arnold, H. E., Kerrison, P., and Steinke, M. (2013), Interacting effects of ocean acidification and warming on growth and DMS-production in the haptophyte coccolithophore Emiliania huxleyi, *Global Change Biology*, *19*(4), 1007-1016, doi:10.1111/gcb.12105.

Barnes, I., Hjorth, J., and Mihalopoulos, N. (2006), Dimethyl sulfide and dimethyl sulfoxide and their oxidation in the atmosphere, *Chemical Reviews*, *106*(3), 940-975, doi:10.1021/cr020529+.

Barton, A. D., Irwin, A. J., Finkel, Z. V., and Stock, C. A. (2016), Anthropogenic climate change drives shift and shuffle in North Atlantic phytoplankton communities, *Proceedings of the National Academy of Sciences of the United States of America*, *113*(11), 2964-2969, doi:10.1073/pnas.1519080113.

Baumann, M. E. M., Brandini, F. P., and Staubes, R. (1994), The influence of light and temperature on carbon-specific DMS release by cultures of Phaeocystis antarctica and three antarctic diatoms, *Marine Chemistry*, *45*(1-2), 129-136, doi:10.1016/0304-4203(94)90097-3.

Behrenfeld, M. J., Moore, R. H., Hostetler, C. A., Graff, J., Gaube, P., Russell, L. M., et al. (2019), The North Atlantic Aerosol and Marine Ecosystem Study (NAAMES): Science Motive and Mission Overview, *Frontiers in Marine Science*, *6*, doi:10.3389/fmars.2019.00122.

Bell, T. G., Porter, J. G., Wang, W.-L., Lawler, M. J., Boss, E., Behrenfeld, M. J., and Saltzman, E. S. (2021), Predictability of Seawater DMS During the North Atlantic Aerosol and Marine Ecosystem Study (NAAMES), *Frontiers in Marine Science*, *7*, 596763, doi:10.3389/fmars.2020.596763.

Bergen, K. J., Johnson, P. A., de Hoop, M. V., and Beroza, G. C. (2019), Machine learning for data-driven discovery in solid Earth geoscience, *Science*, *363*(6433), eaau0323, doi:10.1126/science.aau0323.

Bock, J., Michou, M., Nabat, P., Abe, M., Mulcahy, J. P., Olivié, D. J. L., et al. (2021), Evaluation of ocean dimethylsulfide concentration and emission in CMIP6 models, *Biogeosciences*, *18*(12), 3823-3860, doi:10.5194/bg-18-3823-2021.

Bouillon, R.-C., and Miller, W. L. (2005), Photodegradation of dimethyl sulfide (DMS) in natural waters: Laboratory assessment of the nitrate-photolysis-induced DMS oxidation, *Environmental Science & Technology*, *39*(24), 9471-9477.

Boyce, D. G., Lewis, M. R., and Worm, B. (2010), Global phytoplankton decline over the past century, *Nature*, *466*(7306), 591-596, doi:10.1038/nature09268.

Cameron-Smith, P., Elliott, S., Maltrud, M., Erickson, D., and Wingenter, O. (2011), Changes in dimethyl sulfide oceanic distribution due to climate change, *Geophysical Research Letters*, *38*(7), L07704, doi:10.1029/2011gl047069.

Charette, M. A., Gille, S. T., Sanders, R. J., and Zhou, M. (2013), Southern Ocean natural iron fertilization, *Deep Sea Research Part II: Topical Studies in Oceanography*, *90*, 1-3, doi:10.1016/j.dsr2.2013.04.014.

Charlson, R. J., Lovelock, J. E., Andreaei, M. O., and Warren, S. G. (1987), Oceanic phytoplankton, atmospheric sulphur, cloud albedo and climate, *Nature*, *326*(6114), 655-661, doi:10.1038/326655a0.

Deng, X., Chen, J., Hansson, L.-A., Zhao, X., and Xie, P. (2021), Eco-chemical mechanisms govern phytoplankton emissions of dimethylsulfide in global surface waters, *National Science Review*, *8*(2), nwaa140, doi:10.1093/nsr/nwaa140.

DiTullio, G. R., Grebmeier, J. M., Arrigo, K. R., Lizotte, M. P., Robinson, D. H., Leventer, A., et al. (2000), Rapid and early export of Phaeocystis antarctica blooms in the Ross Sea, Antarctica, *Nature*, *404*(6778), 595-598, doi:10.1038/35007061.

Durack, P. J., Wijffels, S. E., and Matear, R. J. (2012), Ocean salinities reveal strong global water cycle intensification during 1950 to 2000, *Science*, *336*(6080), 455-458, doi:10.1126/science.1212222.

Feng, J., Stige, L. C., Hessen, D. O., Zuo, Z., Zhu, L., and Stenseth, N. C. (2021), A Threshold Sea‐Surface Temperature at 14°C for Phytoplankton Nonlinear Responses to Ocean Warming, *Global Biogeochemical Cycles*, *35*(5), e2020GB006808, doi:10.1029/2020gb006808.

Flombaum, P., Gallegos, J. L., Gordillo, R. A., Rincón, J., Zabala, L. L., Jiao, N., et al. (2013), Present and future global distributions of the marine Cyanobacteria Prochlorococcus and Synechococcus, *Proceedings of the National Academy of Sciences of the United States of America*, *110*(24), 9824-9829.

Flombaum, P., Wang, W.-L., Primeau, F. W., and Martiny, A. C. (2020), Global picophytoplankton niche partitioning predicts overall positive response to ocean warming, *Nature Geoscience*, *13*(2), 116-120.

Forget, G., Campin, J.-M., Heimbach, P., Hill, C. N., Ponte, R. M., and Wunsch, C. (2015), ECCO version 4: An integrated framework for non-linear inverse modeling and global ocean state estimation, *Geoscientific Model Development*, *8*(10), 3071-3104.

Gabric, A. J., Simó, R., Cropp, R. A., Hirst, A. C., and Dachs, J. (2004), Modeling estimates of the global emission of dimethylsulfide under enhanced greenhouse conditions, *Global Biogeochemical Cycles*, *18*(2), GB2014, doi:10.1029/2003gb002183.

Galí, M., Devred, E., Babin, M., and Levasseur, M. (2019), Decadal increase in Arctic dimethylsulfide emission, *Proceedings of the National Academy of Sciences of the United States of America*, *116*(39), 19311-19317, doi:10.1073/pnas.1904378116.

741 Galí, M., Kieber, D. J., Romera-Castillo, C., Kinsey, J. D., Devred, E., Pérez, G. L., et al. (2016),
742 CDOM Sources and Photobleaching Control Quantum Yields for Oceanic DMS Photolysis,
743 *Environmental Science & Technology*, *50*(24), 13361-13370, doi:10.1021/acs.est.6b04278.

744 Galí, M., Levasseur, M., Devred, E., Simó, R., and Babin, M. (2018), Sea-surface
745 dimethylsulfide (DMS) concentration from satellite data at global and regional scales,
746 *Biogeosciences*, *15*(11), 3497-3519, doi:10.5194/bg-15-3497-2018.

747 Galí, M., Lizotte, M., Kieber, D. J., Randelhoff, A., Hussherr, R., Xue, L., et al. (2021), DMS
748 emissions from the Arctic marginal ice zone, *Elementa: Science of the Anthropocene*, *9*(1),
749 doi:10.1525/elementa.2020.00113.

750 Galí, M., and Simó, R. (2015), A meta-analysis of oceanic DMS and DMSP cycling processes:
751 Disentangling the summer paradox, *Global Biogeochemical Cycles*, *29*(4), 496-515,
752 doi:10.1002/2014gb004940.

753 Girard, S., Mallet, V., Korsakissok, I., and Mathieu, A. (2016), Emulation and Sobol' sensitivity
754 analysis of an atmospheric dispersion model applied to the Fukushima nuclear accident, *Journal*
755 *of Geophysical Research: Atmospheres*, *121*(7), 3484-3496, doi:10.1002/2015jd023993.

756 Haaf, D., Six, J., and Doetterl, S. (2021), Global patterns of geo-ecological controls on the
757 response of soil respiration to warming, *Nature Climate Change*, *11*(7), 623-627,
758 doi:10.1038/s41558-021-01068-9.

759 Hayashida, H., Carnat, G., Galí, M., Monahan, A. H., Mortenson, E., Sou, T., and Steiner, N. S.
760 (2020), Spatiotemporal Variability in Modeled Bottom Ice and Sea Surface Dimethylsulfide
761 Concentrations and Fluxes in the Arctic During 1979–2015, *Global Biogeochemical Cycles*,
762 *34*(10), e2019GB006456, doi:10.1029/2019gb006456.

763 Hodshire, A. L., Campuzano-Jost, P., Kodros, J. K., Croft, B., Nault, B. A., Schroder, J. C., et al.
764 (2019), The potential role of methanesulfonic acid (MSA) in aerosol formation and growth and
765 the associated radiative forcings, *Atmospheric Chemistry and Physics*, *19*(5), 3137-3160,
766 doi:10.5194/acp-19-3137-2019.

767 Hoffmann, E. H., Tilgner, A., Schroedner, R., Bräuer, P., Wolke, R., and Herrmann, H. (2016),
768 An advanced modeling study on the impacts and atmospheric implications of multiphase
769 dimethyl sulfide chemistry, *Proceedings of the National Academy of Sciences of the United*
770 *States of America*, *113*(42), 11776-11781, doi:10.1073/pnas.1606320113.

771 Hopkins, F. E., Turner, S. M., Nightingale, P. D., Steinke, M., Bakker, D., and Liss, P. S. (2010),
772 Ocean acidification and marine trace gas emissions, *Proceedings of the National Academy of*
773 *Sciences of the United States of America*, *107*(2), 760-765, doi:10.1073/pnas.0907163107.

774 Hou, L., Dai, Q., Song, C., Liu, B., Guo, F., Dai, T., et al. (2022), Revealing Drivers of Haze
775 Pollution by Explainable Machine Learning, *Environmental Science & Technology Letters*, *9*(2),
776 112-119, doi:10.1021/acs.estlett.1c00865.

777 Huang, B., Zhu, J., Marx, L., Wu, X., Kumar, A., Hu, Z.-Z., et al. (2014), Climate drift of
778 AMOC, North Atlantic salinity and arctic sea ice in CFSv2 decadal predictions, *Climate*
779 *Dynamics*, *44*(1-2), 559-583, doi:10.1007/s00382-014-2395-y.

Hulswar, S., Simó, R., Galí, M., Bell, T. G., Lana, A., Inamdar, S., et al. (2022), Third revision of the global surface seawater dimethyl sulfide climatology (DMS-Rev3), *Earth System Science Data*, *14*(7), 2963-2987, doi:10.5194/essd-14-2963-2022.

Iverson, R., Nearhoof, F., and Andreae, M. (1989), Production of dimethylsulfonium propionate and dimethylsulfide by phytoplankton in estuarine and coastal waters, *Limnology and Oceanography*, *34*(1), 53-67.

Johnson, M. T. (2010), A numerical scheme to calculate temperature and salinity dependent air-water transfer velocities for any gas, *Ocean Science*, *6*(4), 913-932, doi:10.5194/os-6-913-2010.

Keller, M. D., Bellows, W. K., and Guillard, R. R. (1989), Dimethyl sulfide production in marine phytoplankton, in *Biogenic Sulfur in the Environment*, edited by E. S. Saltzman and W. J. Cooper, ACS Publications.

Kettle, A. J., Andreae, M. O., Amouroux, D., Andreae, T. W., Bates, T. S., Berresheim, H., et al. (1999), A global database of sea surface dimethylsulfide (DMS) measurements and a procedure to predict sea surface DMS as a function of latitude, longitude, and month, *Global Biogeochemical Cycles*, *13*(2), 399-444, doi:10.1029/1999gb900004.

Kloster, S., Six, K. D., Feichter, J., Maier-Reimer, E., Roeckner, E., Wetzel, P., et al. (2007), Response of dimethylsulfide (DMS) in the ocean and atmosphere to global warming, *Journal of Geophysical Research: Biogeosciences*, *112*(G3), G03005, doi:10.1029/2006jg000224.

Kwiatkowski, L., Aumont, O., and Bopp, L. (2019), Consistent trophic amplification of marine biomass declines under climate change, *Global Change Biology*, *25*(1), 218-229, doi:10.1111/gcb.14468.

Lana, A., Bell, T. G., Simó, R., Vallina, S. M., Ballabrera-Poy, J., Kettle, A. J., et al. (2011), An updated climatology of surface dimethlysulfide concentrations and emission fluxes in the global ocean, *Global Biogeochemical Cycles*, *25*(1), GB1004, doi:10.1029/2010gb003850.

Levasseur, M. (2013), Impact of Arctic meltdown on the microbial cycling of sulphur, *Nature Geoscience*, *6*(9), 691-700, doi:10.1038/ngeo1910.

Longhurst, A. R. (1998), *Ecological Geography of the Sea*, Academic Press.

Masson-Delmotte, V., Zhai, P., Pirani, A., Connors, S. L., Péan, C., Berger, S., et al. (2021), IPCC, 2021: Climate Change 2021: The Physical Science Basis. Contribution of Working Group I to the Sixth Assessment Report of the Intergovernmental Panel on Climate Change*Rep.*

McCoy, D. T., Burrows, S. M., Wood, R., Grosvenor, D. P., Elliott, S. M., Ma, P. L., et al. (2015), Natural aerosols explain seasonal and spatial patterns of Southern Ocean cloud albedo, *Science Advances*, *1*(6), e1500157, doi:10.1126/sciadv.1500157.

McParland, E. L., and Levine, N. M. (2018), The role of differential DMSP production and community composition in predicting variability of global surface DMSP concentrations, *Limnology and Oceanography*, *64*(2), 757-773, doi:10.1002/lno.11076.

Molnar, C. (2020), *Interpretable machine learning*, Lulu. com.

Murdoch, W. J., Singh, C., Kumbier, K., Abbasi-Asl, R., and Yu, B. (2019), Definitions, methods, and applications in interpretable machine learning, *Proceedings of the National*

Academy of Sciences of the United States of America, *116*(44), 22071-22080, doi:10.1073/pnas.1900654116.

Nöthig, E.-M., Bracher, A., Engel, A., Metfies, K., Niehoff, B., Peeken, I., et al. (2015), Summertime plankton ecology in Fram Strait—a compilation of long- and short-term observations, *Polar Research*, *34*(1), doi:10.3402/polar.v34.23349.

Novak, G. A., Fite, C. H., Holmes, C. D., Veres, P. R., Neuman, J. A., Faloona, I., et al. (2021), Rapid cloud removal of dimethyl sulfide oxidation products limits SO2 and cloud condensation nuclei production in the marine atmosphere, *Proceedings of the National Academy of Sciences of the United States of America*, *118*(42), e2110472118, doi:10.1073/pnas.2110472118.

Omori, Y., Tanimoto, H., Inomata, S., Wada, S., Thume, K., and Pohnert, G. (2015), Enhancement of dimethylsulfide production by anoxic stress in natural seawater, *Geophysical Research Letters*, *42*(10), 4047-4053, doi:10.1002/2015gl063546.

Orkney, A., Platt, T., Narayanaswamy, B. E., Kostakis, I., and Bouman, H. A. (2020), Bio-optical evidence for increasing Phaeocystis dominance in the Barents Sea, *Philosophical Transactions of the Royal Society A: Mathematical, Physical and Engineering Sciences*, *378*(2181), 20190357, doi:10.1098/rsta.2019.0357.

Osman, M. B., Das, S. B., Trusel, L. D., Evans, M. J., Fischer, H., Grieman, M. M., et al. (2019), Industrial-era decline in subarctic Atlantic productivity, *Nature*, *569*(7757), 551-555, doi:10.1038/s41586-019-1181-8.

Park, K. T., Yoon, Y. J., Lee, K., Tunved, P., Krejci, R., Ström, J., et al. (2021), Dimethyl Sulfide‐Induced Increase in Cloud Condensation Nuclei in the Arctic Atmosphere, *Global Biogeochemical Cycles*, *35*(7), e2021GB006969, doi:10.1029/2021gb006969.

Qin, Y., Ye, J., Ohno, P., Liu, P., Wang, J., Fu, P., et al. (2022), Assessing the Nonlinear Effect of Atmospheric Variables on Primary and Oxygenated Organic Aerosol Concentration Using Machine Learning, *ACS Earth and Space Chemistry*, doi:10.1021/acsearthspacechem.1c00443.

Quinn, P. K., and Bates, T. S. (2011), The case against climate regulation via oceanic phytoplankton sulphur emissions, *Nature*, *480*(7375), 51-56, doi:10.1038/nature10580.

Quinn, P. K., Coffman, D. J., Johnson, J. E., Upchurch, L. M., and Bates, T. S. (2017), Small fraction of marine cloud condensation nuclei made up of sea spray aerosol, *Nature Geoscience*, *10*(9), 674-679, doi:10.1038/ngeo3003.

Reichstein, M., Camps-Valls, G., Stevens, B., Jung, M., Denzler, J., Carvalhais, N., and Prabhat (2019), Deep learning and process understanding for data-driven Earth system science, *Nature*, *566*(7743), 195-204, doi:10.1038/s41586-019-0912-1.

Reigstad, M., Wassmann, P., Wexels Riser, C., Øygarden, S., and Rey, F. (2002), Variations in hydrography, nutrients and chlorophyll a in the marginal ice-zone and the central Barents Sea, *Journal of Marine Systems*, *38*(1-2), 9-29, doi:10.1016/s0924-7963(02)00167-7.

Rivero-Calle, S., Gnanadesikan, A., Del Castillo, C. E., Balch, W. M., and Guikema, S. D. (2015), Multidecadal increase in North Atlantic coccolithophores and the potential role of rising CO(2), *Science*, *350*(6267), 1533-1537, doi:10.1126/science.aaa8026.

Sallee, J. B., Pellichero, V., Akhoudas, C., Pauthenet, E., Vignes, L., Schmidtko, S., et al. (2021), Summertime increases in upper-ocean stratification and mixed-layer depth, *Nature*, *591*(7851), 592-598, doi:10.1038/s41586-021-03303-x.

Schoemann, V., Becquevort, S., Stefels, J., Rousseau, V., and Lancelot, C. (2005), Phaeocystis blooms in the global ocean and their controlling mechanisms: a review, *Journal of Sea Research*, *53*(1-2), 43-66, doi:10.1016/j.seares.2004.01.008.

Sheng, J.-X., Weisenstein, D. K., Luo, B.-P., Rozanov, E., Stenke, A., Anet, J., et al. (2015), Global atmospheric sulfur budget under volcanically quiescent conditions: Aerosol-chemistry-climate model predictions and validation, *Journal of Geophysical Research: Atmospheres*, *120*(1), 256-276, doi:10.1002/2014jd021985.

Sigmund, G., Gharasoo, M., Hüffer, T., and Hofmann, T. (2020), Deep Learning Neural Network Approach for Predicting the Sorption of Ionizable and Polar Organic Pollutants to a Wide Range of Carbonaceous Materials, *Environmental Science & Technology*, *54*(7), 4583-4591, doi:10.1021/acs.est.9b06287.

Simó, R., and Pedrós-Alió, C. (1999), Role of vertical mixing in controlling the oceanic production of dimethyl sulphide, *Nature*, *402*(6760), 396-399, doi:10.1038/46516.

Six, K. D., Kloster, S., Ilyina, T., Archer, S. D., Zhang, K., and Maier-Reimer, E. (2013), Global warming amplified by reduced sulphur fluxes as a result of ocean acidification, *Nature Climate Change*, *3*(11), 975-978, doi:10.1038/nclimate1981.

Smith, W. O., Codispoti, L. A., Nelson, D. M., Manley, T., Buskey, E. J., Niebauer, H. J., and Cota, G. F. (1991), Importance of Phaeocystis blooms in the high-latitude ocean carbon cycle, *Nature*, *352*(6335), 514-516, doi:10.1038/352514a0.

Sobol', I. M. (2001), Global sensitivity indices for nonlinear mathematical models and their Monte Carlo estimates, *Mathematics and Computers in Simulation*, *55*(1), 271-280, doi:10.1016/S0378-4754(00)00270-6.

Sobol', I. M., and Myshetskaya, E. E. (2008), Monte Carlo estimators for small sensitivity indices, *Monte Carlo Methods and Applications*, *13*(5-6), 455-465, doi:10.1515/MCMA.2007.023.

Stefels, J. (2000), Physiological aspects of the production and conversion of DMSP in marine algae and higher plants, *Journal of Sea Research*, *43*(3-4), 183-197.

Stefels, J., Steinke, M., Turner, S., Malin, G., and Belviso, S. (2007), Environmental constraints on the production and removal of the climatically active gas dimethylsulphide (DMS) and implications for ecosystem modelling, *Biogeochemistry*, *83*(1-3), 245-275, doi:10.1007/s10533-007-9091-5.

Sunda, W., Kieber, D., Kiene, R., and Huntsman, S. (2002), An antioxidant function for DMSP and DMS in marine algae, *Nature*, *418*(6895), 317-320.

Sunda, W. G., Hardison, R., Kiene, R. P., Bucciarelli, E., and Harada, H. (2007), The effect of nitrogen limitation on cellular DMSP and DMS release in marine phytoplankton: climate feedback implications, *Aquatic Sciences*, *69*(3), 341-351, doi:10.1007/s00027-007-0887-0.

Tagliabue, A., Mtshali, T., Aumont, O., Bowie, A. R., Klunder, M. B., Roychoudhury, A. N., and Swart, S. (2012), A global compilation of dissolved iron measurements: focus on

distributions and processes in the Southern Ocean, *Biogeosciences*, *9*(6), 2333-2349, doi:10.5194/bg-9-2333-2012.

Tesdal, J.-E., Christian, J. R., Monahan, A. H., and Salzen, K. v. (2016), Evaluation of diverse approaches for estimating sea-surface DMS concentration and air–sea exchange at global scale, *Environmental Chemistry*, *13*(2), 390-412, doi:10.1071/EN14255.

Toole, D. A., Kieber, D. J., Kiene, R. P., White, E. M., Bisgrove, J., del Valle, D. A., and Slezak, D. (2004), High dimethylsulfide photolysis rates in nitrate-rich Antarctic waters, *Geophysical Research Letters*, *31*(11), n/a-n/a, doi:10.1029/2004gl019863.

Toole, D. A., and Siegel, D. A. (2004), Light-driven cycling of dimethylsulfide (DMS) in the Sargasso Sea: Closing the loop, *Geophysical Research Letters*, *31*(9), n/a-n/a, doi:10.1029/2004gl019581.

Vallina, S. M., and Simó, R. (2007), Strong relationship between DMS and the solar radiation dose over the global surface ocean, *Science*, *315*(5811), 506-508, doi:10.1126/science.1133680.

Vallina, S. M., Simó, R., Gassó, S., de Boyer-Montégut, C., del Río, E., Jurado, E., and Dachs, J. (2007a), Analysis of a potential "solar radiation dose-dimethylsulfide-cloud condensation nuclei" link from globally mapped seasonal correlations, *Global Biogeochemical Cycles*, *21*(2), GB2004, doi:10.1029/2006gb002787.

Vallina, S. M., Simo, R., and Manizza, M. (2007b), Weak response of oceanic dimethylsulfide to upper mixing shoaling induced by global warming, *Proceedings of the National Academy of Sciences of the United States of America*, *104*(41), 16004-16009, doi:10.1073/pnas.0700843104.

Veres, P. R., Neuman, J. A., Bertram, T. H., Assaf, E., Wolfe, G. M., Williamson, C. J., et al. (2020), Global airborne sampling reveals a previously unobserved dimethyl sulfide oxidation mechanism in the marine atmosphere, *Proceedings of the National Academy of Sciences of the United States of America*, *117*(9), 4505-4510, doi:10.1073/pnas.1919344117.

Vogt, M., O'Brien, C., Peloquin, J., Schoemann, V., Breton, E., Estrada, M., et al. (2012), Global marine plankton functional type biomass distributions: Phaeocystis spp., *Earth System Science Data*, *4*(1), 107-120, doi:10.5194/essd-4-107-2012.

Wagener, T., and Pianosi, F. (2019), What has Global Sensitivity Analysis ever done for us? A systematic review to support scientific advancement and to inform policy-making in earth system modelling, *Earth-Science Reviews*, *194*, 1-18, doi:10.1016/j.earscirev.2019.04.006.

Wang, S., Elliott, S., Maltrud, M., and Cameron-Smith, P. (2015), Influence of explicit Phaeocystis parameterizations on the global distribution of marine dimethyl sulfide, *Journal of Geophysical Research: Biogeosciences*, *120*(11), 2158-2177, doi:10.1002/2015jg003017.

Wang, S., Maltrud, M. E., Burrows, S. M., Elliott, S. M., and Cameron‐Smith, P. (2018), Impacts of Shifts in Phytoplankton Community on Clouds and Climate via the Sulfur Cycle, *Global Biogeochemical Cycles*, *32*(6), 1005-1026, doi:10.1029/2017gb005862.

Wang, W.-L., Song, G., Primeau, F., Saltzman, E. S., Bell, T. G., and Moore, J. K. (2020), Global ocean dimethyl sulfide climatology estimated from observations and an artificial neural network, *Biogeosciences*, *17*(21), 5335-5354, doi:10.5194/bg-17-5335-2020.

Wittek, B., Carnat, G., Delille, B., Tison, J.-L., and Gypens, N. (2020), Dimethylsulfoniopropionate (DMSP) and dimethylsulfoxide (DMSO) cell quotas variations

arising from sea ice shifts of salinity and temperature in the Prymnesiophyceae Phaeocystis antarctica, *Environmental Chemistry*, *17*(7), doi:10.1071/en19302.

Woodhouse, M. T., Mann, G. W., Carslaw, K. S., and Boucher, O. (2013), Sensitivity of cloud condensation nuclei to regional changes in dimethyl-sulphide emissions, *Atmospheric Chemistry and Physics*, *13*(5), 2723-2733, doi:10.5194/acp-13-2723-2013.

Woolf, D. K. (1997), Bubbles and their role in gas exchange, in *The Sea Surface and Global Change*, edited by P. S. Liss and R. A. Duce, pp. 173-206, Cambridge University Press, Cambridge, doi:10.1017/CBO9780511525025.007.

Yang, H., Lohmann, G., Krebs‐Kanzow, U., Ionita, M., Shi, X., Sidorenko, D., et al. (2020), Poleward Shift of the Major Ocean Gyres Detected in a Warming Climate, *Geophysical Research Letters*, *47*(5), e2019GL085868, doi:10.1029/2019gl085868.

Zhang, X. H., Liu, J., Liu, J., Yang, G., Xue, C. X., Curson, A. R. J., and Todd, J. D. (2019), Biogenic production of DMSP and its degradation to DMS-their roles in the global sulfur cycle, *Science China Life Science*, *62*(10), 1296-1319, doi:10.1007/s11427-018-9524-y.

Zheng, G., Li, X., Zhang, R. H., and Liu, B. (2020), Purely satellite data-driven deep learning forecast of complicated tropical instability waves, *Science Advances*, *6*(29), eaba1482, doi:10.1126/sciadv.aba1482.

Zhu, C., and Liu, Z. (2020), Weakening Atlantic overturning circulation causes South Atlantic salinity pile-up, *Nature Climate Change*, *10*(11), 998-1003, doi:10.1038/s41558-020-0897-7.

Zindler, C., Bracher, A., Marandino, C. A., Taylor, B., Torrecilla, E., Kock, A., and Bange, H. W. (2013), Sulphur compounds, methane, and phytoplankton: interactions along a north–south transit in the western Pacific Ocean, *Biogeosciences*, *10*(5), 3297-3311, doi:10.5194/bg-10-3297-2013.

Zindler, C., Marandino, C. A., Bange, H. W., Schütte, F., and Saltzman, E. S. (2014), Nutrient availability determines dimethyl sulfide and isoprene distribution in the eastern Atlantic Ocean, *Geophysical Research Letters*, *41*(9), 3181-3188, doi:10.1002/2014gl059547.

References From the Supporting Information

Beale, R., M. Johnson, P. S. Liss, and P. D. Nightingale (2014), Air–Sea Exchange of Marine Trace Gases, in *Treatise on Geochemistry (Second Edition)*, edited by H. D. Holland and K. K. Turekian, pp. 53-92, Elsevier, Oxford.

Galí, M., E. Devred, M. Levasseur, S.-J. Royer, and M. Babin (2015), A remote sensing algorithm for planktonic dimethylsulfoniopropionate (DMSP) and an analysis of global patterns, *Remote Sensing of Environment*, *171*, 171-184, doi:10.1016/j.rse.2015.10.012.

Nightingale, P. D., G. Malin, C. S. Law, A. J. Watson, P. S. Liss, M. I. Liddicoat, J. Boutin, and R. C. Upstill-Goddard (2000), In situ evaluation of air-sea gas exchange parameterizations using novel conservative and volatile tracers, *Global Biogeochemical Cycles*, *14*(1), 373-387, doi:10.1029/1999gb900091.

978 Sathyendranath, S., V. Stuart, A. Nair, K. Oka, T. Nakane, H. Bouman, M. H. Forget, H. Maass,
979 and T. Platt (2009), Carbon-to-chlorophyll ratio and growth rate of phytoplankton in the sea,
980 *Marine Ecology Progress Series*, *383*, 73-84, doi:10.3354/meps07998.

981